Review

Synthesis, technological prospects and applications of MXene in biomedicine, supercapacitors and sensors: A review

Nujud Badawi M.[1],[*], M. Bhuyan[2],[*], Namrata Agrawal[3], Yogesh Kumar[4]

[1] University of Hafr Al-Batin College of Science, Hafer Al-Batin 39921, Saudi Arabia

[2] Institute of Physics, Sachivalaya marg, Bhubaneswar 751005, India

[3] Department of Physics, Swami Shraddhanand College, University of Delhi, New Delhi 110036, India

[4] Department of Physics, ARSD College, University of Delhi, Delhi 110021, India

* Corresponding authors: Nujud Badawi M., nujuds@uhb.edu.sa; M. Bhuyan, bunuphy@um.edu.my

Abstract: MXenes are one of the most important classes of materials discussed worldwide by many researchers of diverse fields for diverse applications in recent years. It is a nanomaterial with a wide range of applications due to its multiple forms and structures with fascinating properties, for example, high surface area and porosity, biocompatibility, ease of fictionalizing with various active chemical moieties, benefit of high metallic conductivity, activated metallic hydroxide sites, and sensitivity to moisture. MXenes have great chances for potential applications in environmental issues, water purification, biological applications, and energy storage devices and sensors. MXenes show great selectivity towards the absorption of heavy metals and a good capability to reduce chemical and biological pollutants present in the water. The present review article critically analyzed advancements in water purification using the adsorption and reduction abilities of MXenes and their composites. The mechanism of various procedures, important challenges, and associated problems using MXene and their composites are discussed in detail. The future research directions can be extracted from this article efficiently and comprehensively. The energy storage issues of rechargeable lithium-ion batteries, batteries other than lithium-ion batteries, and electrochemical capacitors are also discussed in detail.

Keywords: 2D materials; MXene; energy storage; batteries; capacitors

1. Introduction

In 2011, a new type of two-dimensional substance called MXene was discovered for the first time. The MXene family sparked intense interest in research across many disciplines due to its diverse chemical composition and excellent physical and chemical properties, particularly in the areas of energy storage, the environment, catalysis, and biomedical applications, the latter of which, in particular, is experiencing rapid growth. Since graphene's exfoliation [1,2], a lot of attention has been paid to other 2D layered materials [3,4] because of their exceptional electrical, mechanical, and optical capabilities. Most studied examples of 2D materials other than graphene include transition metal dichalcogenides [4,5], phosphorene [6,7], and their derivatives. In recent years [6], a family of 2D-layered compounds known as "MXenes" has attracted a great deal of interest from the scientific community due to their unusual structural and electrical properties, which make them applicable to a wide range of fields.

MXenes are compounds produced by the chemical delamination of ternary (or quaternary) layered carbides or nitrides. The unique properties of the MXene family

are due to their electrical structures, atomic stacking, synthetic methods, surface terminal groups, and peculiar bonding, which consists of metallic and covalent connections. Despite MXenes rising star power, there is a dearth of comprehensive information on them.

Many sensors [2–4], as well as portable and wearable electronic devices [5–7], have emerged to sense and interact with physical worlds to foster the development of a smarter life with the vigorous rise of the internet of things (IoT) and the great improvement of the reliability of wireless communication protocols [1]. Despite this, a reliable power supply [8–10] requires the successful integration of on-chip energy-storage units with novel electronic devices due to the intermittent nature of renewable resources (wind [11], solar [12], tidal [13], and geothermal energy [14]). Conventional micro-batteries have a high energy density [15] and can keep devices running for a while, but they are unable to meet the requirement of rapid power delivery in applications where battery replacement is impractical [16]. Micro-supercapacitors (MSCs) have gained widespread interest as a micro-battery substitute because of their fascinating long lifetime, high power density, and fast charging rate [17]. However, their progress in microelectronics is hampered by their low power and energy density [18].

With the rapid development of biomedicine and the attractive physiochemical properties of two-dimensional materials, many researchers have focused on the biomedical applications of two-dimensional materials, such as hexagonal boron nitrides (h-BN), graphene and its derivatives, transition metal oxides (TMOs), layered double hydroxides (LDHs), and MXenes. MXenes have more functional groups on their surface, allowing for greater versatility in modification than most other 2D materials. MXenes are useful for biomedical applications due to their hydrophilicity, compositional versatility, and the presence of full metal atomic layers. Another advantage is that MXenes can be mass-produced at low cost. Bioimaging, antimicrobials, biosensors, drug delivery, tissue engineering, and a wide range of therapeutics are just some of the ways MXenes have been put to use in the medical field so far (**Figure 1a**) [19]. Because of their high near-infrared light absorption and conversion efficiency, MXenes have found applications in photothermal therapy for tumour ablation. This form of treatment is highly effective in targeting cancer cells while causing minimal collateral damage to healthy tissue. In addition, bioimaging can be used in real-time to track the tumour's location as contrast chemicals are administered during cancer treatment. In addition, the modified MXenes can also carry anticancer medications and release pharmaceuticals in a specific manner. Photothermal therapy, chemotherapy, and real-time bioimaging monitoring have considerably increased the success rate of cancer treatment thus far. As a bonus, MXenes are proving to be promising raw materials for developing biocompatible tools for easy, rapid detection of biological events [19].
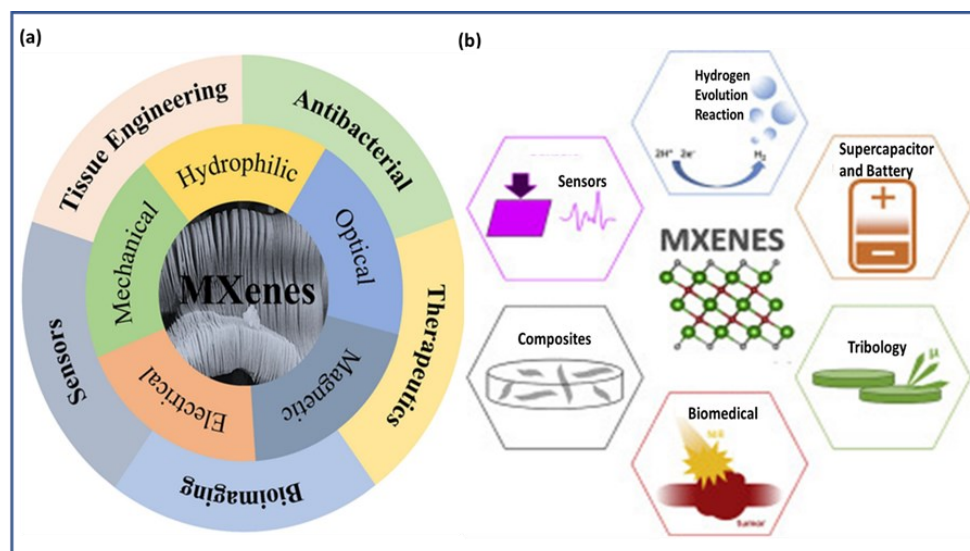
Figure 1. (a) Properties and biomedical applications of MXenes [19]; **(b)** MXenes in a wide range of applications [20].

The purpose of this study was to analyze and remark on the most important basic and technological aspects of MXenes about their structure, electronics, properties, applications, and devices (see **Figure 1b**) [20]. The history of MXenes' creation is presented first, followed by examples of MXene production, structure, and characteristics, surface modification schemes, biomedical applications, cytotoxicity, and biocompatibility. We have examined the key features and properties of MXenes. The present status, trends and future possibilities in various fields, such as energy, electronics, biomedicine, etc., have been critically examined. Finally, current challenges and future potential applications of MXene have been discussed.

2. Logic of MXene

New 2D transition metal carbides, nitrides, and carbonitrides called MXenes (pronounced "machines") were first fabricated by wind [11], solar [12], tidal [13], and geothermal energy [14]. Hydrofluoric acid (HF) was used at room temperature to selectively etch the "A" (Al atoms) in layered hexagonal ternary carbide, Ti_3AlC_2, to produce the first MXene made of 2D titanium carbide (Ti_3C_2). From the precursor MAX phase ($M_{n+1}AX_n$), MXenes can be constructed with the general formula $M_{n+1}X_nT_x$ ($n = 1$–3), where M is an early transition metal, X is carbon and/or nitrogen, A is an element from groups 12 to 16, T is the surface termination groups like fluorine (–F), oxygen (=O), chlorine (–Cl), and hydroxyl (–OH), and x is the number of surface functionalities [21]. There is a strong M-X bond and a comparatively weak M-A bond in the MAX phase, where an A layer is sandwiched by octahedral $M_{n+1}X_n$ [22]. Elements that produce MAX phases ($M_{n+1}AX_n$) are denoted in bold in **Figure 2** [23]. Depending on the n value in MXenes ($M_{n+1}X_nT_x$), the interlayer spacing can be anywhere from 0.1 to 1.0 nm [8].
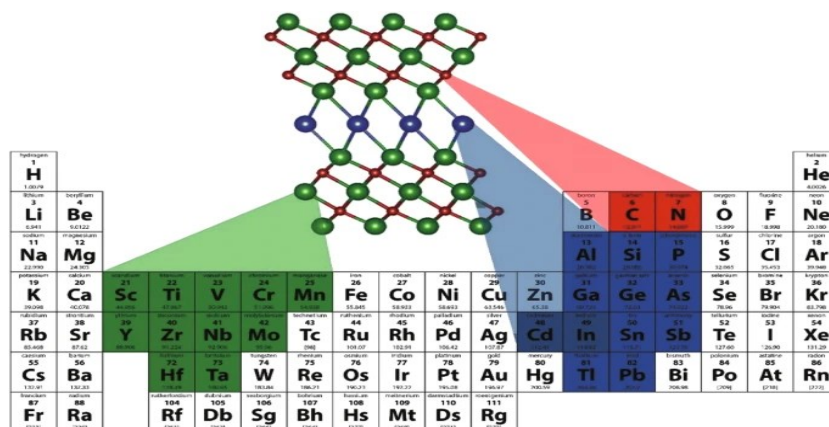
Figure 2. Elements in the periodic table that are known to form $M_{n+1}AX_n$ phases. Reprinted with the permission from Ref [23].

3. Synthesis methodologies of MXene: Procedures and structures

About 30 different compositions of MXenes have been described in the literature, all of which have been synthesized from MAX phase precursors, with the addition of two or more transition metals to the M layers as the primary route to do so [20]. In particular, MXenes based on titanium, such as $Ti_3C_2T_x$ and Ti_2CT_x, are widely used for ecological purposes [1,17]. Other MXene structures, such as those including nitride and carbonitride, have also found use outside of the realm of carbides [23]. MXenes' distinct layered structures and 2D morphology make them an ideal candidate for use in composites, which can be utilized to improve the properties of other materials [8]. Preparing a sample for synthesis involves taking a few parameters into account, like safety, cost, procedures, instruments (such as monitors and gauges), and control systems. Etching, exfoliation, and chemical vapour deposition (CVD) are the three most common approaches to MXene production. Etching and exfoliation are examples of top-down processes, while chemical vapour deposition, the template method, and plasma-enhanced pulsed laser deposition are examples of bottom-up techniques.

The most popular method for synthesizing 2D MXenes is the top-down etching of 'A' from MAX phases ($M_{n+1}AX_n$), where M is an early transition metal; A is one of numerous elements (Al, Si, P, S, Ga, Ge, As, Cd, In, Sn, Tl, or Pb); X is C, N or both; and n is 1–4. Metallic bonds are typical between *M* and *A*, but covalent, ionic, or metallic bonds can exist between M and X [19]. As a result, it is difficult to break the M-A connection using mechanical shearing or direct exfoliation. Etchants, such as HF, can, however, etch it selectively. Two processes are required in the synthesis of MXenes [20,24] (**Figure 3**) [25]: First, selective etching of the A element from a precursor (MAX phases or other layered ceramics); second, delamination to obtain a single-layer MXene. However, the manufacturing of MXenes for energy storage applications has not been thoroughly addressed using these methods. The processes of MXene manufacturing are explained in greater detail below. Each MXene has a mother MX phase from which it is created, where "M" represents an early transition metal, "A" represents a group 13 or 14 element, "X" represents carbon or nitrogen, and "n" ranges from 1 to 3 [21].
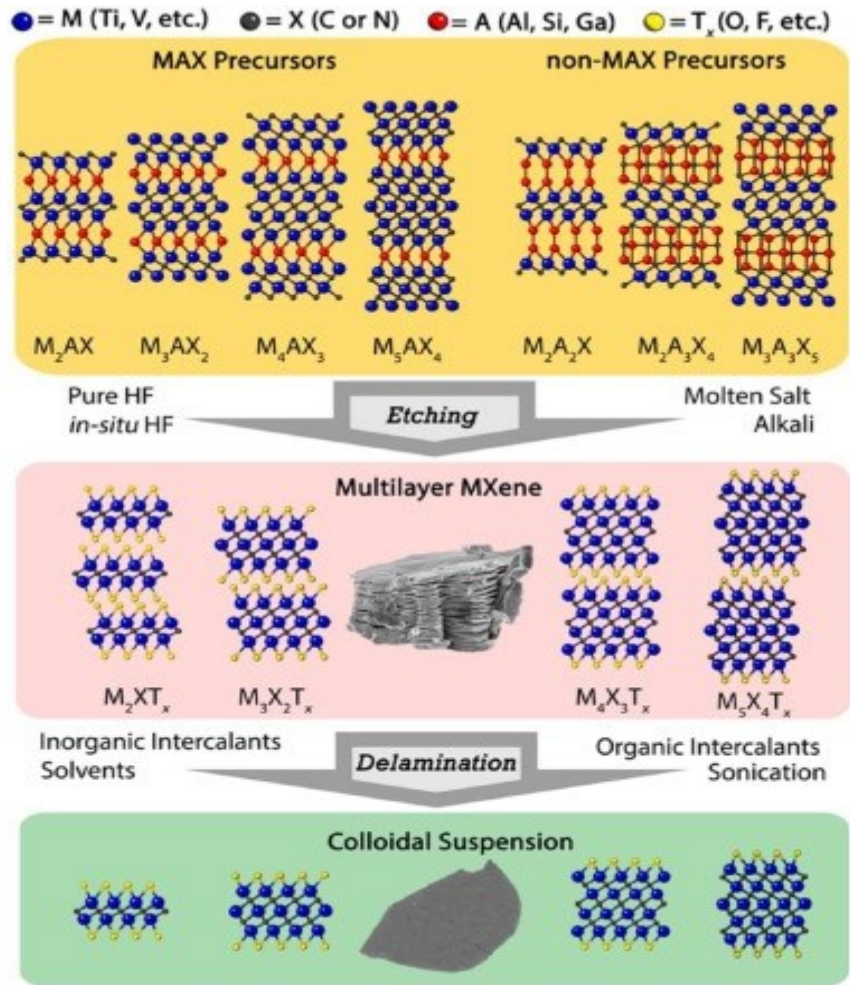
Figure 3. Synthesis of Mxene—selective etching of MAX and non-MAX phases to form multilayered MXenes, followed by delamination (chemical/mechanical) to produce a colloidal suspensionof single-layered MXene [25].

MXenes. In the top-down process, MXenes were synthesized from the bulk by a two-stage procedure: chemical etching and delamination [8,26]. To remove the interleaved layers of 'A' atoms from the bulk ceramic, an etchant is utilized to cleave the M-A metallic connection. The aggregated nanosheets are then delaminated via liquid-phase exfoliation [8], tetrapropylammonium hydroxide (TPAOH) intercalation [27,28], or ultrasonication [26]. In **Figure 4a** [29], a schematic depicting the steps involved in creating MXene is given. To prevent the dangers of fluorine-based etchants, fluorine-free techniques are also used [30]. Bottom-up methods often employ CVD technology, which works upwards from the atomic or molecular level [31]. Both top-down synthesis and bottom-up approaches can be used to create
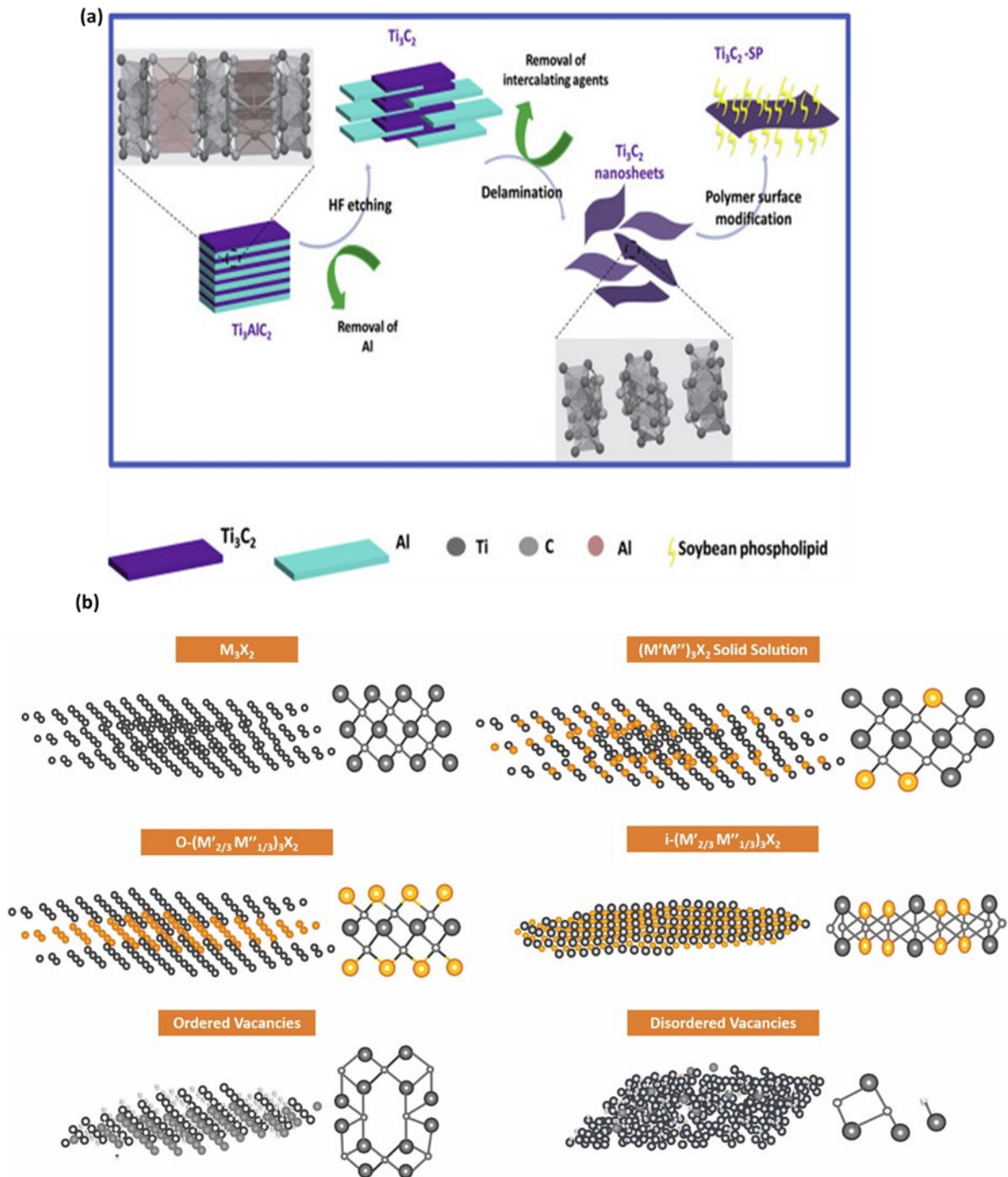
Figure 4. (a) Fabrication of 2D ultrathin Ti_3C_2 nanosheets by etching, delamination, and surface modification along with its crystal structure [29]; **(b)** different structures of MXenes [27].

4. Simulation-based studies on MXene structures

To complement experimental studies and get a more in-depth understanding of MXene structures, computer simulations are frequently used. MXenes typically end with surface groups, including –F, –OH, and –O, following exfoliation from the MAX phase. The usefulness of such structures is determined by the relationships among their features and characteristics [26]. There are three possible configurations of MXenes, all of which correspond to the parent MAX phases and have a single

metal in the M site: M_2C, M_3C_2, and M_4C_3, where M is an early transition metal, A is a particular element from groups 13 or 14, X is carbon or nitrogen, and n is a number from one to four. The A element must be carefully removed from a MAX phase or other stacked precursor (such as MO_2Ga_2C). In MAX phases, X atoms fill octahedral sites in an otherwise hexagonally stacked M layer with P63/MMC symmetry. As a result, the A and M elements form metallic bonds. $M_{n+1}X_n$ layers and MXenes containing ordered double-transition metals, like (Cr_2V) C_2 and (MO_2Ti_2) C_3, are interwoven throughout the "A" element [29]. Computer modelling has helped disclose the structures of MXenes and has also aided in the discovery of new, stable MXenes. There are six distinct MXene structures: (1) Nb_4C_3 and Ti_2C are examples of mono-M components; (2) $(Cr, V)_3C_2$ and $(Ti, V)_3C_2$ are examples of solid solutions; (3) ordered out-of-plane two-fold M components have one transition metal (typically Cr and Mo) filling the outer layers and the other the focus layers (Ta and Nb); (4) ordered in-plane two-fold M components have the distinguishing M components arranged in the basal plane, such as in [22,27,29–32]. Structures of different MXenes are shown in **Figure 4b**.

The surface terminations (–F, –OH, and –O) group linked to M atoms give MXene its chemical formula, $M_{n+1}X_nT_z$ (1 n 3). **Figure 5a** [22] depicts the steps required to prepare MXene. A typical schematic diagram is depicted in **Figure 5b** [33], representing the process of synthesizing MXenes from MAX phases.
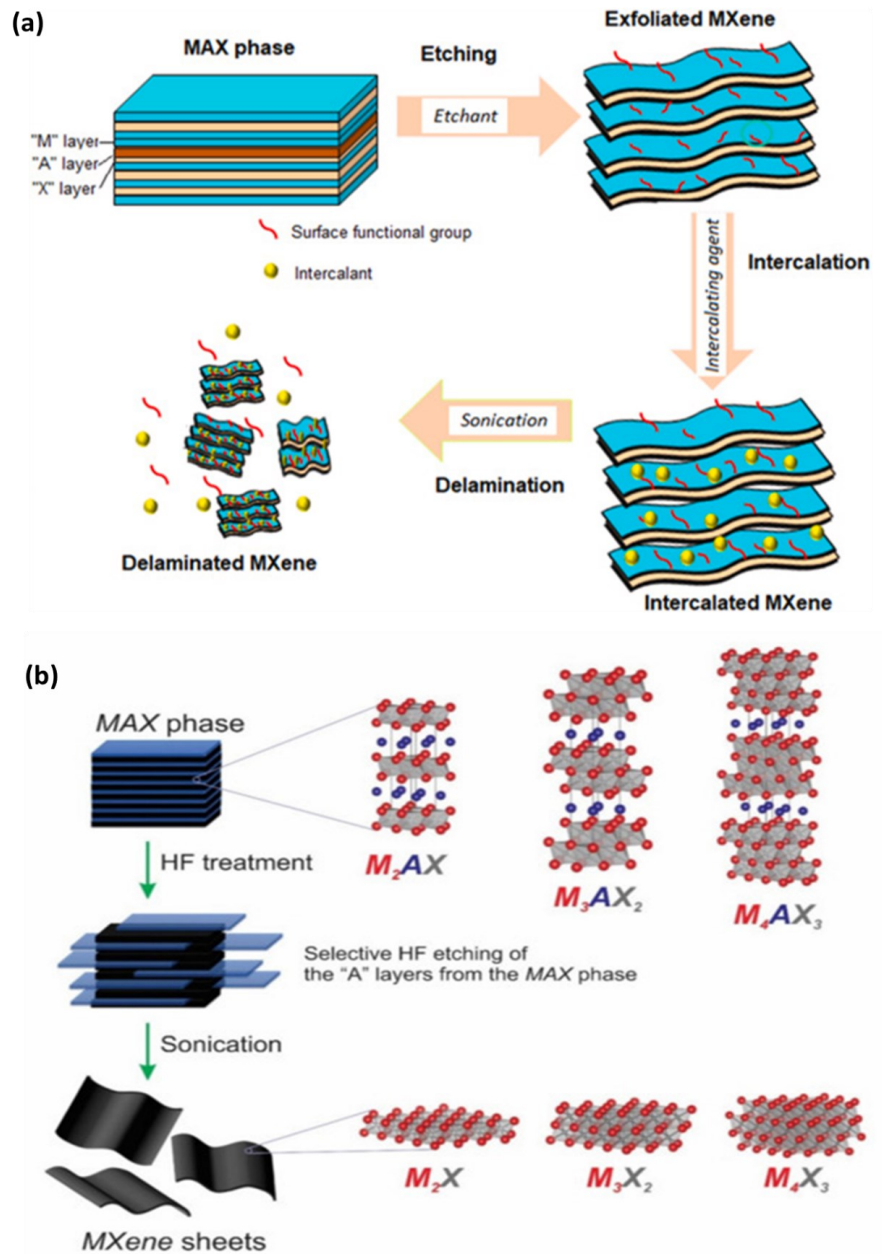
Figure 5. (a) MXenes, derived from the parent layered solids MAX phases [22]; **(b)** the schematic diagram represents the process of synthesizing MXenes from MAX phases. Reproduced with permission from [33].

5. Applications

5.1. Prospects of MXenes in biological applications

The promising results of MXenes in stem cell-based tissue treatments and the material sciences make it reasonable to expect future multi-tasking biomedical therapies to be based on their unique properties [33]. Titanium carbide (Ti_3C_2) MXene nanofibers were used to create smart biomaterials for tissue engineering and cell culture in one study. Fabrication of hydrophilic composite nanofibers via electrospinning and doping was carried out by Chen et al. [34]. The MXene nanofiber composites' surface functional groups were considered to foster healthy

cellular environments. Bone marrow-derived mesenchymal stem cells (BMSCs) were used to analyse the biochemically representative characteristics, and the resulting MXene composite nanofibers showed good biocompatibility and significantly improved cellular activity, as well as boosting BMSC differentiation to osteoblasts.

Smart biomaterials, which have many desirable biological characteristics, are very useful in tissue engineering and repair procedures [35]. Because of their immunomodulatory properties, which selectively reduced the activation of human CD4+IFN-+ T-lymphocytes while stimulating the expansion of immunosuppressive $CD_4+CD_{25}+FoxP_3+$regulatory T-cells in a stimulated lymphocyte population, two-dimensional structures with BMSC biocompatibility could stimulate fibroblasts derived from bone marrow-derived stem cells (BMSCs) for post-injury tissue repair. [35,36]. The incorporation of Ti_3C_2MXene QDs (quantum dots (MQDs) sensor) into a chitosan hydrogel resulted in the creation of a 3D platform with enhanced physicochemical characteristics, which can facilitate stem cell trafficking and tissue restoration. The resultant composite hydrogel was both injectable and thermos-sensitive, and it showed excellent conductivity [37]. In a similar line, biocompatible Ti_3C_2Tz-enhanced poly (lactic acid) nanocomposite membranes were created by mediating the interface between the hydrophobic poly (lactic acid) matrix and the Ti_3C_2Tz nanosheets. These membranes achieved an optimized tensile strength of 72 MPa, which is approximately 33% greater than a pure poly (lactic acid) membrane [37,38]. Therefore, Ti_3C_2Tz insertion into the membrane might improve its biological characteristics, including osteogenic differentiation, proliferation, and in vitro adhesion of MC3T3-E1 murine preosteoblasts.

MXenes' exceptional properties, which include hydrophilicity, high electronic conductivity, and adsorptive, reductive, and antibacterial properties, make them well-suited for a wide range of ecological uses. The adaptability of MXenes makes them desirable for a wide range of uses. Their chemical stability, ion intercalation, and adjustable bang gaps suggest catalysis and energy storage applications like fuel cells, hydrogen storage, and lithium-ion batteries (LIBs), while their high Young's modulus, good electrical conductivity, and surface chemistry alteration are appealing for the creation of composites.

5.2. MXenes for environmental and water treatment applications

5.2.1. H_2O_2 oxidation activated by MXene-based materials

Hydrogen peroxide (H_2O_2) oxidation has attracted much attention in the removal of pollutants [36], where Fe^{2+} can act as a catalyst to form free radicals [36,39]. 2D MXene has a layered structure and surface electronegativity. Metal particles can be loaded onto the surface and layered surfaces of 2D MXene [24,40]. In addition, 2D MXene can also degrade metal nanoparticles and inhibit the aggregation of metal nanoparticles [41]. Interestingly, metal particle-loaded 2D MXene has a larger surface area and better pore structure than pure 2D MXene. The pores in the composite can serve as microreactors for H_2O_2 activation. Magnetic nanoscale zero-valent iron particles (nZVI)@Ti_3C_2 nanosheets could remove 91.1% of ranitidine in 30 min [42]. Therefore, 2D MXene-supported metal particles can be

considered a good catalyst to activate H_2O_2 to degrade organic pollutants.

Wu et al. [43] developed a nanoplatform based on multimodal TMO connecting ultrathin Ti_3C_2 nanosheets to self-assembled $MnFe_2O_4$ nanoparticles using chitosan as a chemical cross-linking agent to form an interfacial Schottky junction, Ti_3C_2@Chitosan-$MnFe_2O_4$(TC@Ch-MFO). This led to an improvement in reactive oxygen species (ROS) production and optimization of biocompatibility. This heterojunction could control the catalysis of H_2O_2 to produce O_2 and deplete excess glutathione levels in the hypoxic tumor microenvironment, so that under near-infrared stimulation, the cyclization was completed by the Fenton reaction. TC@ChMFO also provided a multifunctional nanoplatform for photothermal therapy by introducing an effective photothermal agent, Ti_3C_2. Additionally, it integrated visualization with T1- and T2-weighted magnetic resonance imaging simultaneously (see **Figure 6a**) [43]. As the toxicity of TC@ChMFO to normal tissues is negligible, this platform might provide new insights into the development of multimodal synergistic nanoplatforms for biological applications.
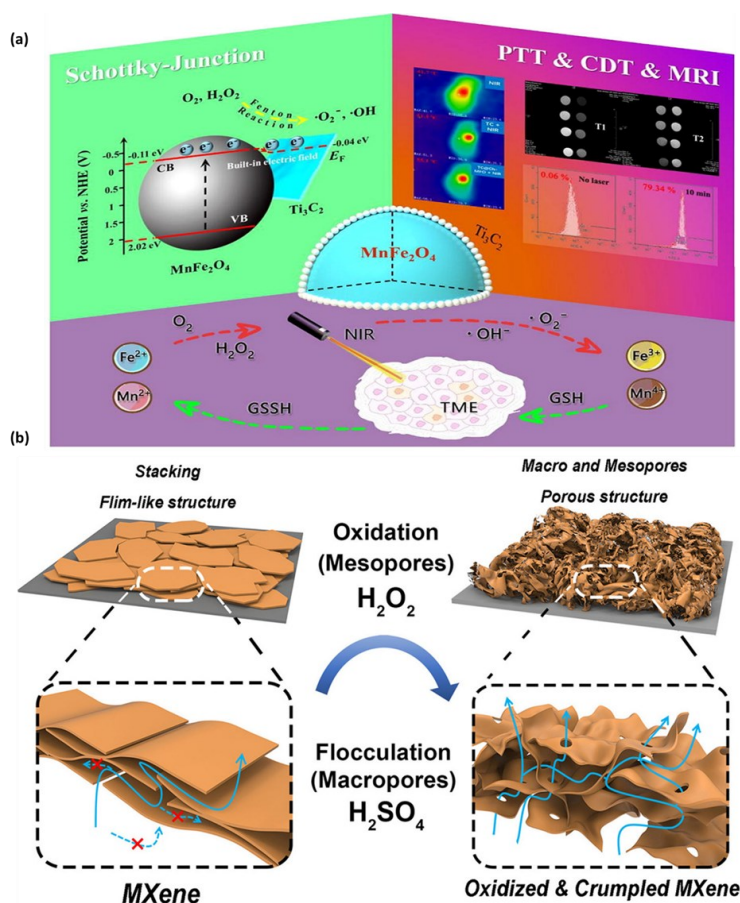
Figure 6. (a) MXene-based Schottky junctions self-assembled transition metal oxides for near-infrared radiation to modify the tumor microenvironment and enhance CDT/PTT/MRI activation [43]; **(b)** oxidized MXene co-wrinkled multi scale porous structure [44].

Lee et al. [44] proposed a new method to produce MXene oxidative wrinkled multiscale porous structures through a sequential process involving partial oxidation with H_2O_2 as agglomeration in acid (see **Figure 6b**). These processes lead to the

simultaneous formation of mesopores caused by oxidation and macropores due to shrinkage patterns. The specific surface area of oxidatively co-degraded MXene (72 m^2/g) was found to be five times that of pure MXene. The efficiency of the performance (307 F/g at 20 mV/s in 1 M H_2SO_4) and the capacity of the scan (225 F/g at 100 mV/s) were also found to be better than in pure MXene. Additionally, 87.6% of capacity was retained after 6000 cycles. This was due to the structure of porous, oxidized, folded MXene. Here, the diffusion of ions through mesopores was promoted, while folded macropores prevented restacking.

The performance and mechanism of Ti_3C_2 MXene-modified Fe^{3+}/hydrogen peroxide system in dark light and visible light were compared in detail, and a new standard for coating Fe^{3+} reactions and reductions of MXene was proposed by Xu et al. [45]. Taking Bisphenol A (BPA) as the target pollutant, the degradation effect of BPA in the Fe^{3+}/H_2O_2 system was improved after adding MXene in the dark. The degradation of BPA in 12.5 min under visible light was ≥95%, which was 6 times higher than in the dark. Fe^{2+} was identified as a useful element for the activation of H_2O_2 to form OH. It was found that MXene formed a complex with Fe^{3+}. MXene reacted with Fe^{3+}, breaking the TiC bond and activating the Fe^{3+}/Fe^{2+} cycle. MXene used photogenerated electrons to promote chemical reactions under light. OH and O_2 were found to be the main reactive oxygen species in light, while OH was the main reactive oxygen species in light (see **Figure 7a**). Thus, MXene could utilize O_2 to produce O_2 and promote the Fe^{3+}/Fe^{2+} cycle in light. This work provided a theoretical basis for the combination of visible light catalysis and the higher oxidation process of Ti_3C_2 MXene.
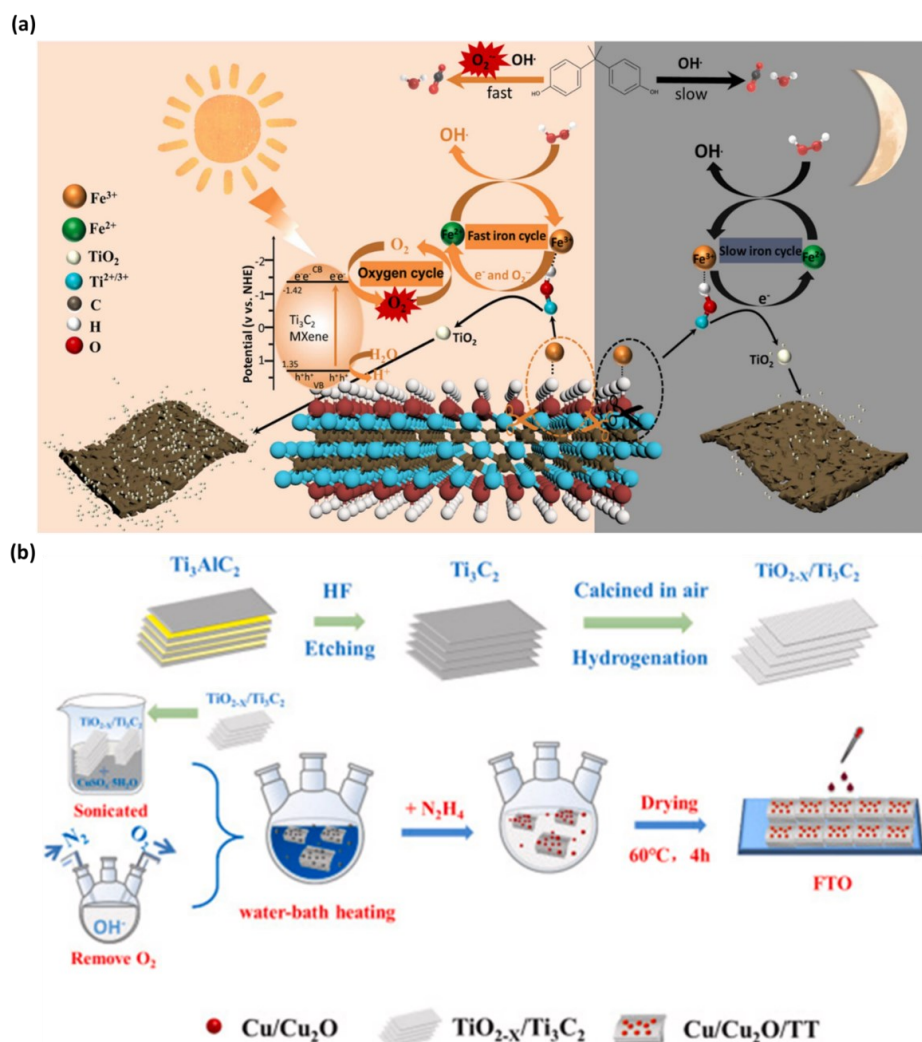
Figure 7. (a) Ti_3C_2 MXene promotes Fe^{3+}/H_2O_2 Fenton oxidation: comparison of the process under dark light and visible light [45]; **(b)** the fabrication process of the $Cu/Cu_2O/TiO_{2-X}$ electrode [46].

To detect H_2O_2, Li et al. [46] used in-situ produced TiO_{2-X} nanoparticles to modify Cu/Cu_2O nanoparticles on Ti_3C_2 MXene to form heterojunctions via a single-step hydrothermal process. The produced $Cu/Cu_2O/TiO_{2-X}/Ti_3C_2$($Cu/Cu_2O/TT$) was found to have a linear range of 28.328 mM, a sensitivity of 312 $\mu A\ mM^{-1}\ cm^{-2}$ and detection limit of 0.42 μM. The synergistic effect of Cu/Cu_2O nanoparticles and TiO_{2-X}/Ti_3C_2 heterojunction not only improved the electron transfer and electrocatalytic activity but also increased the strength of the target molecules of the catalyst due to the abundance of extended catalytic sites. Therefore, compared to TiO_2X/Ti_3C_2, the detection limit of $Cu/Cu_2O/TT$ was low, its reaction faster, and its sensitivity five times higher. Also, $Cu/Cu_2O/TT$ exhibited excellent photoelectrochemical sensing performance in detecting H_2O_2 with a low detection limit, long-term stability, repeatability, and selectivity. The fabrication process of the $Cu/Cu_2O/TT$ electrode followed by Li et al. [46] is shown in **Figure 7b**.

Iron particles deposited on the 2D MXene surface may exhibit multiple reaction zones. 2D MXene can facilitate the electrical transfer of magnetic materials. In addition, there are many hydrophilic functional groups (such as OH, COOH, and

CHO) on the surface of MXene/nanoscale zero-valent iron particle nanosheets, designed to promote H_2O_2 activation [43]. Zhu et al. [47] used $Ti_3C_2T_X$ to develop a sensitive and enzyme-free electrochemical sensing interface to detect H_2O_2 simply and practically. Prussian blue (PB) was electrochemically deposited on the surface of the glassy carbon electrode (GCE). Chitosan (CS) and MXene were degraded on the PB modified GCE surface. Simple MX/CS/PB/GCE detection interface demonstrated good electrochemical detection performance and good selection for H_2O_2 with a low limit (4 nM) and a wide linear range from 50 nM to 667 μM.

The light-driven magnetic MXene microrobot (MXeBOT) was developed as a moveable stage for the removal and degradation of bisphenol A (BPA) by Dekanovsky et al. [48]. A second control motor composed of embedded Fe_2O_3 nanoparticles (NPs) for magnetic push assisted the MXeBOT. Grafted bismuth nanoparticles acted as co-catalysts. It was investigated how BPA concentration and the chemical composition of the swimming environment affected the stability and reusability of MXeBOTs. MAXBOT could remove/degrade approximately 60% of BPA in just 10 minutes and approximately 100% in 1 hour. More than 86% of BPA mineralized within 1 h. Using Bi/Fe/MXeBOTs for the photocatalytic degradation of BPA demonstrated a significant advantage in converting BPA into CO_2 and H_2O [49].

5.2.2. Other advanced water remediation applications of MXenes

MXene and its compounds have also proven effective in other environmental applications such as membranes, capacitive deionization, and anti-bacterial agents. MXene is a promising product for water filtration due to its hydrophilicity, high surface area, and excellent electrical properties [48]. Molecules can be separated based on the size of the surface layer and the interaction with the MXene layer. In recent years, MXenes have been used in a variety of environmental applications for the treatment of contaminated groundwater and municipal wastewater, including desalination, outperforming the most widely used material in all regions [50]. MXene composites can adsorb a variety of organic and inorganic compounds and can undergo Faradaic capacitive deionization (CDI) when used in electrochemical applications. This method overcomes the concentration polarization limit of conventional CDI electrodes, greatly reducing the energy required and providing a solution for low-energy desalination of brackish water. Researchers provide an updated review of MXene and MXene mixtures for water purification and desalination applications. Kinetics and isotherms were examined, and the effects of water composition and activity discussed. Based on the literature review, the application of MXene in CDI, pervaporation desalination, and photothermal desalination have been studied. The impact of water composition and performance on recovery efficiency and long-term use has also been highlighted (see **Figure 8a**) [51].
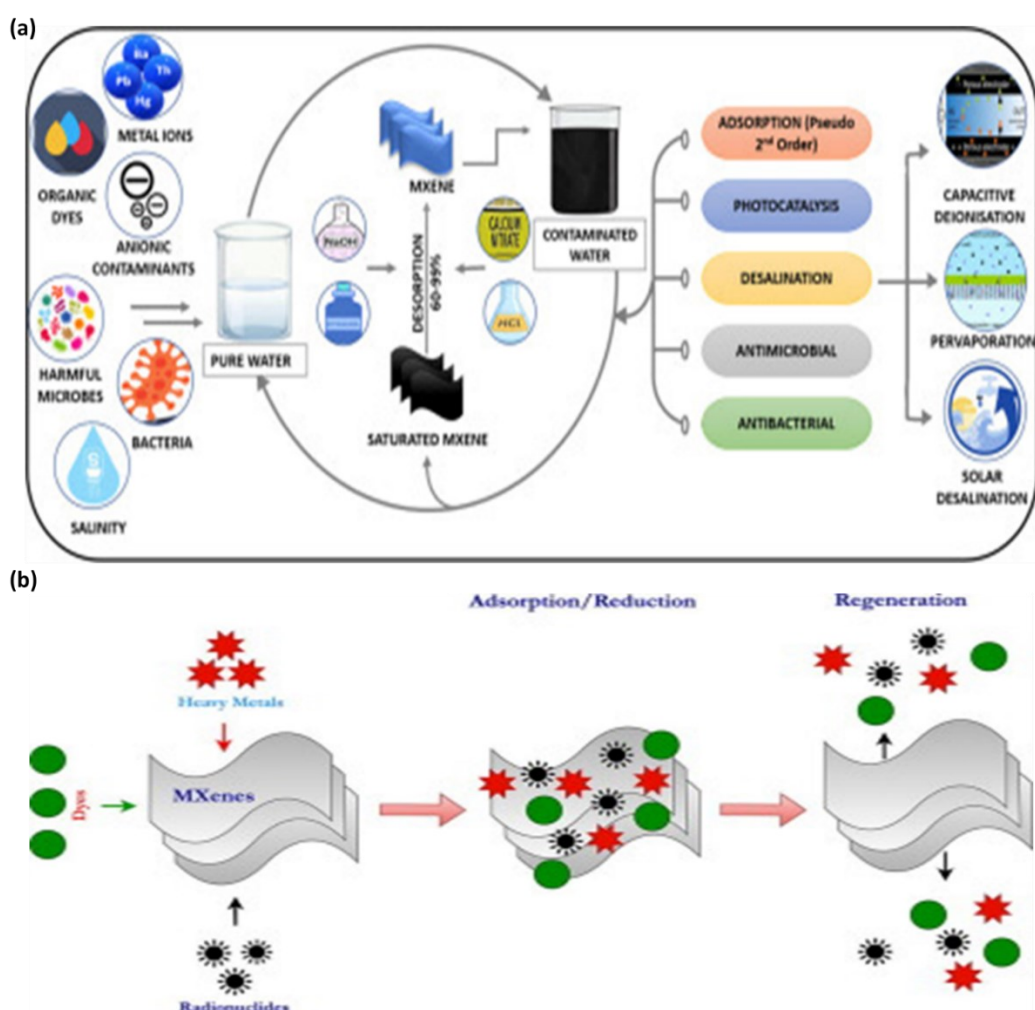
Figure 8. (a) Use of MXenes in water purification and energy-saving desalination [51]; **(b)** MXenes (2D metal carbides) as nanomaterials for water purification [49].

There is an interest in using MXene and its derivatives in water purification due to their unique properties. MXene has high electrical conductivity and hydrophilicity, as well as outstanding adsorption, reduction, and disinfection properties. In particular, $Ti_3C_2T_X$ and its compounds are widely used in water purification to remove various contaminants such as dyes, radionuclides, and heavy metals. Ihsanullah [49] evaluated the effectiveness of MXene and MXene-based mixtures in removing various pollutants from water, focusing on heavy metals, dyes, and radionuclides. The role of the MXene structure in the contaminant elimination process and the regeneration were reviewed and analyzed (see **Figure 8b**). The properties of MXene, such as high electricity, hydrophilicity, and catalytic activity, have attracted increasing research attention in environmental remediation and water purification applications [50]. Reports are available on recent advances in the synthesis and use of MXenes as adsorbents, desalination membranes, electrochemical deionization electrodes, and catalysts or antimicrobial agents for water purification and other environmental treatment. The challenges and opportunities have also been highlighted for advanced 2D materials by discussing experimental efforts to investigate MXenes for water use, biocompatibility, and environmental impact. Due to their unique mechanical, chemical, and electrical

properties, many successful experiments have been carried out on the use of MXenes in water purification and environmental remediation applications. However, more efforts are needed to solve the stability, biocompatibility, and reusability issues of MXenes in aqueous environments. MXenes are reported to be used for pollutant adsorption/remediation, photodegradation, membrane separation, etc.

The increase in pollutants such as air pollution, organic dyes, chemicals, and pesticides released into the water due to population and the global economy has become the most important health problem in the world [51]. Magnetic MXene nanocomposites have many attractive and successful applications due to their unique properties, ease of production, cost-effective preparation, and excellent capability to degrade water and wastewater pollutants. These compounds offer exciting new opportunities for many applications, such as biosensors, cancer therapy, measurement systems, and especially water purification. Researchers are studying magnetic MXene nanocomposites to remove contaminants from ambient water. The use of magnetic nanomaterials for water treatment, the applications and implications of MXene in degrading water and wastewater pollutants, and the role of magnetic-MXene nanocomposites in water treatment have been studied and discussed (**Figure 9a**) [52].
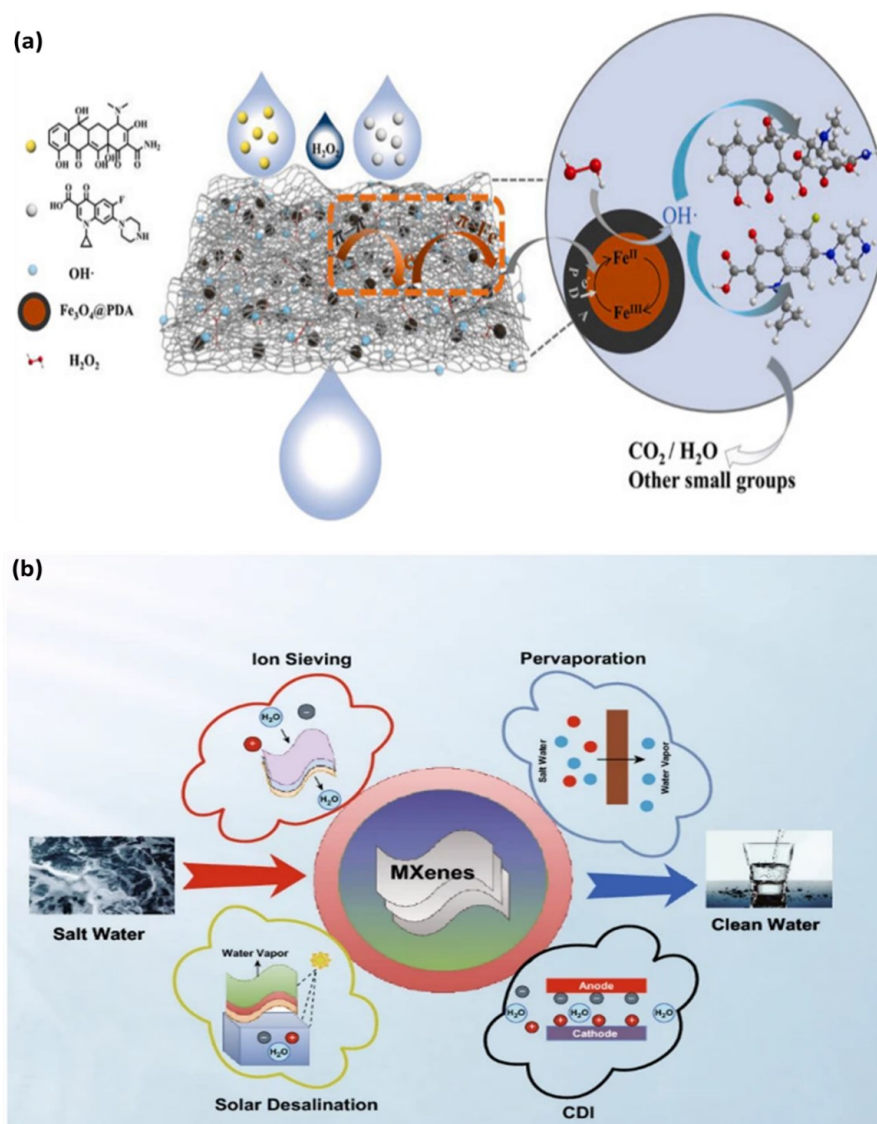
Figure 9. (a) Magnetic-MXene-based nanocomposites for water and wastewater treatment [52]; **(b)** advanced applications of Mxenes in CDI, solar desalination, ion sieving and pervaporation [53].

The advantages of MXene, such as high surface area, high metal conductivity, easy functionalization, biocompatibility, active metal hydroxide surface, and hydrophilicity, make it a good candidate for energy storage, catalysis, sensors, electronics, and environmental application. Due to their good physical and chemical properties and wide range of chemical properties, MXenes have attracted attention in water purification and desalination applications in recent years. Ihsanullah studied the advances in the synthesis of MXenes and MXene-based compounds for seawater desalination. The desalination potential of MXenes was described in detail, focusing on ion screen membranes, capacitive deionization, and solar desalination. The ion removal process and the recycling potential of MXene were also documented to provide insight into the process [53].

MXene has also emerged as a strong candidate for oil/water separation and photocatalytic environmental remediation applications (see **Figure 9b**) [53]. The ability to reduce organic molecules and some cations is a unique property that makes

MXene the best choice for future water purification applications [12]. Due to its hydrophilicity, high conductivity, high adsorption capacity for anions and cations, and tunable surface, MXene can also be used as a new electrode material for CDI applications [54]. The solar and evaporative desalination properties of MXene have also been investigated in various studies [55]. The rapid development of the economy causes serious water pollution and poses a threat to the environment. Currently, heterogeneous Fenton oxidation has attracted widespread attention due to its high efficiency and simple operation. Hydrogen peroxide and persulfate are two oxidants used in Fenton-like processes.

5.3. MXene-based battery

Significant efforts have been devoted to the development of electronic devices with excellent electrical properties and high energy density for energy storage and conversion. 2D materials show great potential in energy storage due to their unique properties. MXenes have excellent properties when used as electrodes for lithium-based batteries. Tang et al. have discussed the developments in MXene and MXene-based composites in terms of synthesis strategies, morphology engineering, physical/chemical attributes, and their use in lithium-ion batteries and lithium-sulfur batteries [56].

5.3.1. MXeneforlithiumbatteries

Lithium batteries are one of the most common types of batteries because they are the engines of modern electronic devices. Lithium batteries are currently used in mobile phones, computers, small cars, airplanes, and home appliances. Lithium's high electropositivity and flexibility make it better than hydrogen [57]. Lithium-based cathodes have problems such as short life, low charge, toxicity, unstable electrolyte, high cost, high self-discharge, and poor specific energy. Anodes made of materials such as graphite, lithium, soft carbon, and tin have problems such as dendrites, low energy density, cracking/dissolution, and voltage fluctuations [58]. Therefore, it is necessary and urgent to produce good electrodes for these batteries. MXene is considered an effective material due to its large surface area, electrical conductivity, tunable thermal conductivity, and chemical stability. Rechargeable lithium-ion batteries (LIBs) have provided much-needed applications in electric vehicles and consumer electronics due to their high energy density and reduced storage capacity. In particular, research on LIBs focuses on their applications in small electronic devices by increasing energy density and reducing the footprint during fast charging [56]. MXene can not only produce lithium-ion batteries but also can produce lighter fuel than lithium ion.

Deng tested MXene as a LIB anode material and found it good due to its high specific surface area, weak interlayer strength, open structure, and surface functional groups [59]. Since MXene consists of functional groups M (when the substituted metal is), X (C and/or N), and T (functional groups O, OH, and F), it is possible to use many substituents for the treatment. goods. For example, the specific potential of different MXenes follows the order $Ti_2C < Nb_2C < V_2C$, with both Nb_2C and V_2C exhibiting higher activity [1]. In addition, the difference between different MXenes is also different. This shows the difference between MXenes for anodes or cathodes.

Additionally, work groups often have different characteristics; for example, bare MXene is magnetic, while active MXene is a semiconductor material. They may also interfere with lithium absorption and transport [54]. Nonnatural functional groups (e.g., chlorine) may be beneficial to MXene by hardening the surface and reducing the interaction of natural OH and F functional groups [55]. Even if the "M" stoichiometry is the same type and prepared by the manufacturing process, the capacity of the lithium-ion battery will be directly affected due to the difference in surface properties. Generally speaking, Ti2CTx has a higher surface energy than Ti3C2TX, which tends to reduce the lattice parameter k and thus inhibit the addition of lithium ions [59].

Lithium-ion MXene/metal electrodes:

The electrode material must have excellent electrical conductivity and be able to withstand high temperatures without cracking or breaking. Nowadays, metal electrodes such as titanium, aluminum, magnesium, copper, silver, zinc, and platinum face many problems. Corrosion, cracking, and low energy density are associated with intrinsic metallic electrodes. Due to the excellent properties of MXene, some researchers have mixed metal electrodes with MXene to improve its electrochemical behavior.

Mxene has a significant problem that affects its performance, such as the aggregation problem of MXene flakes [60]. A simple and effective way to solve this problem is to provide MXene hybrid composites produced with suitable materials such as silicon, tin, different nanocarbon fillers, metal oxides, phosphorus, metal sulfides, and double-layer oxides. The MXene surface is modified in many aspects, including decoration with silicon- and tin-based nanoparticles, bonding the network with carbon nanofillers, and creating heterostructures between graphene and MXene layers. These hybrid materials have high ion energy, high lithium-ion emissivity, and conductivity, in addition to extraordinary capacity. According to the current situation, lithium-ion battery electrode materials should help in improving the electrical properties of batteries, making them more efficient than before. MXene-based hybrid nanostructured materials provide insight into future challenges and guide in finding new materials to be used in future energy applications.

Since the discovery and development of graphene [60], 2D materials and the study of their properties have attracted widespread attention in materials science [34]. In recent years, 2D transition metal carbides, nitrides, and carbonitrides (MXenes for short) have been rapidly developed since the discovery of Ti_3C_2 in 2011 [35]. MXene is prepared by selectively etching individual atomic layers (called MAX phases) in a precursor layer [60].

The general structure of the MAX phase is $M_{n+1}AX_n$ ($n = 1, 2, 3$), where M represents the early transition metal (M = Ti, Sr, V, Cr, Ta, Nb, Zr, Mo, or Hf), and A represents group sp elements (IIIA or IVA only), X represents C or N, and both [39,61]. The MAX phase can be said to be a symbiotic structure in which tightly packed planar atom layers and hexagonal MX layers are stacked alternately. **Figure 10** shows the classical configuration of the MAX system (using Ti_2AlC as an example) [62]. In this structure, MX bonds are mostly ionic/covalent bonds, and all MA bonds are metal bonds [38]. Therefore, the MX bond is stronger than the MA bond and enables the removal of the A layer from the lamellar layer. However,

unlike the weak van der Waals interlayer interactions between graphite and transition metal dichalcogenides, the MA bond is very strong, resulting in detachment of the MX layer from the MAX strength; this is not easily achieved by direct cleavage or ultrasonication techniques. Due to the different properties and strengths of M-X and MA bonds, it is possible to select the appropriate chemical in the process. This leaves a stable chemical structure of the volume near $M_{n+1}X_nT_x$ (T, F, OH, O, etc.), representing the functional group on the surface, near MXene (**Figure 10a**) [62]. The interactions between MXene layers are mainly hydrogen bonds and van der Waals bonds. Water, cations, DMSO, TBAOH, etc. are added to different parts of MXene. After sonication, the MXene layer becomes a suspension.
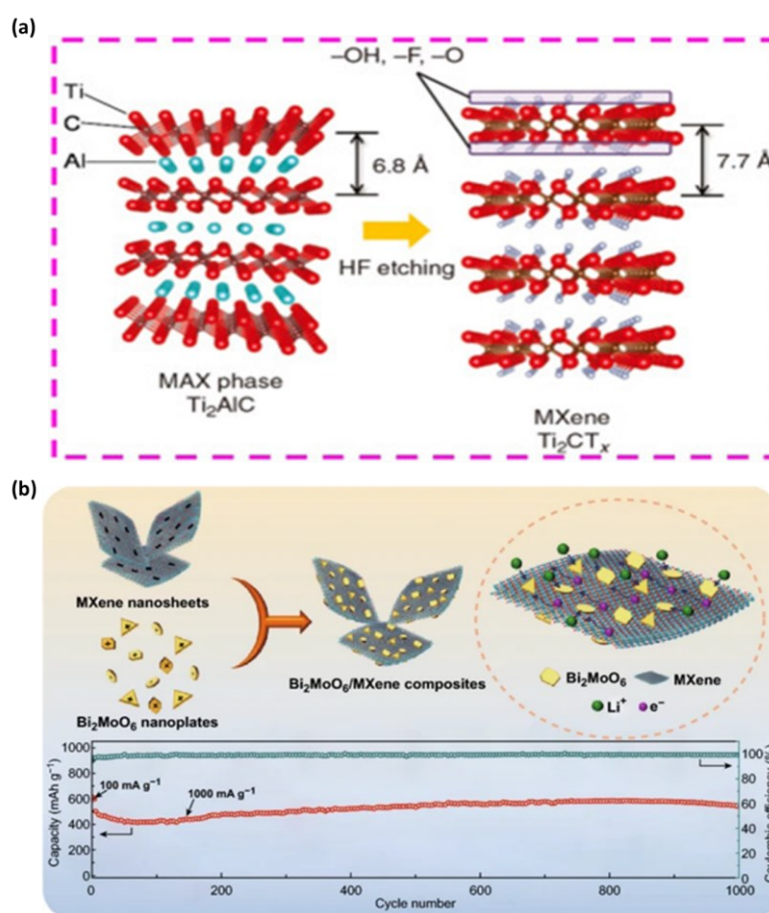

Figure 10. Schematic illustration for the formation of Ti_2CTx MXene from Ti_2AlC phase. **(a)** Reproduced with permission [61]; **(b)** plate-to-layer Bi_2MoO_6/MXene-heterostructured anode for lithium-ion batteries [62].

Due to the low electrical conductivity of Bi_2MoO_6 and the large volume expansion/contraction during charging and discharging, appropriate modification is essential to solve these problems. To overcome the issues, Zhang et al. [62] prepared the plate-to-layer Bi_2MoO_6/Ti_3C_2Tx (MXene) heterostructure by electrostatically assembling positively charged Bi_2MoO_6 nanosheets onto negatively charged MXene nanosheets. MXene nanosheets in heterostructure provided a highly conductive substrate to support and anchor Bi_2MoO_6 nanosheets, thereby increasing electrical conductivity and structure stability (see **Figure 10b**). When the mass fraction of

MXene was optimized to 30%, the Bi_2MoO_6/MXene heterostructure exhibited a specific capacity of 692 mAh g^{-1} at 100 mA g^{-1} after 200 cycles. A 99.6% Coulomb efficiency was achieved with 545.1 mAhg^{-1} at 1 Ag^{-1} after 1000 cycles. The research resulted not only in providing high-performance lithium materials but also presented an idea to create heterostructures by modifying various metal oxides of MXene nanosheets and using them as lithium-ion batteries [62]. Zou et al. [63] synthesized a MXene/Ag composite product ($Ti_3C_2(OH)_{0.8}F_{1.2}$) by directly reducing $AgNO_3$ aqueous solution in the presence of MXene. The results demonstrated that the reduction of Ag in MXene solutions was associated with the presence of low-valence Ti. The recovery capacity at 1 ℃ was 310 mAhg^{-1}, at 10 ℃ it was 260 mAhg^{-1} and the recovery capacity at 50 ℃ was 150 mAhg^{-1}. Moreover, the composite could withstand more than 5000 cycles at 1 to 50 ℃ without decay (see **Figure 11a**).
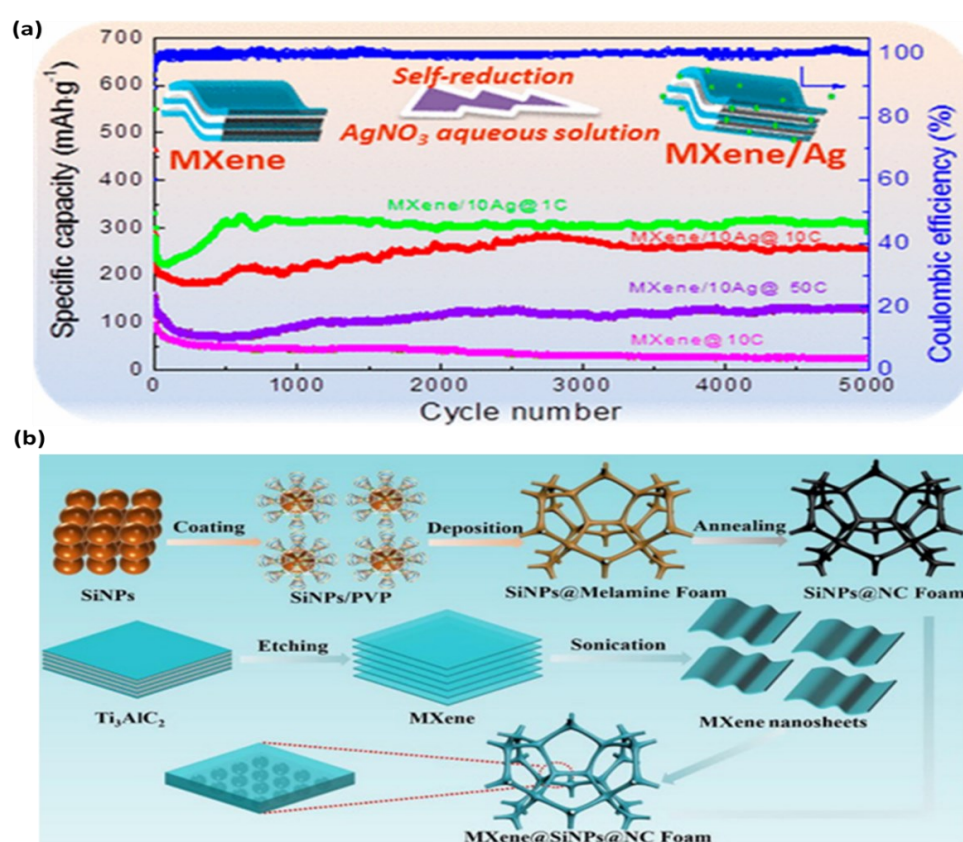

Figure 11. (a) Synthesis of MXene/Ag composites for high-speed lithium storage with ultra-long cycle life [63]; **(b)** schematic diagram of the preparation process of MXene@SiNPs@NC foam composites [64].

Metal-based anode materials such as Sb, Sn, and Bi have received great attention in battery applications due to their high electrical conductivity and high energy density. However, the large volume expansion during the alloying process makes the work very fast. Tian et al. synthesized Sb, Sn, and Bi on MXene sheets via a simple one-step electrodeposition process in a green ethylene glycol system. A strong, flexible, self-contained, and binder-free anode for potassium-ion batteries was prepared. The coating ensured a short diffusion for potassium ions and provided a buffer for the volume change during potassiumization/depotassiumization.

Efficient and flexible MXene materials could then be used as current generators, providing wide electrical paths to facilitate the transport of electricity while cycling and adapting to changing volumes. MXene@Sb resulted in a high reversible capacity of 516.8 mAhg^{-1}, a peak value of 270 mAhg^{-1} at 500 mA g^{-1}, with the fading of only 0.042% per cycle [64].

Lithium-ion MXene/silicon electrode.

Organo-silicon electrodes are one of the best energy storage electrodes due to their unique capacity, non-toxicity, and raw materials. However, silicon expands in volume during cycling, resulting in poor electrochemical cycling performance [65]. The volume expansion that occurs during lithiation/delithiation is the cause of cracking and breakage in the electrode. The combination of silicon and MXene can be used to produce excellent electrochemical electrodes for lithium-ion batteries. The improved cycling performance of silicon/MXene electrodes can be attributed to the excellent thermal stability of MXene. Titanium-based MXene ($Ti_3C_2T_X$) nanosheets have become useful materials for low-voltage electronics (Si) due to their unique charge (lithium) storage capacity and rich abundance of silicon (Si). $Si/Ti_3C_2T_X$ composite material has been shown to have a wide and stable cycle time, good performance, and high economic value. To better understand and improve the electrochemical performance of composites, a review by Jiang et al. focused on the electrochemical processes occurring in Si/MXene composites [65]. Silicon (Si) is one of the most promising materials for lithium-ion batteries (LIB) due to its unique properties. However, low transmission efficiency and large voltage fluctuations block the development of silicon-based anodes. Zhang et al. [66] created a 3D structure containing silicon nanoparticles (SiNPs) anchored on nitrogen-doped carbon (NC) foam and coated with an MXene layer (MXene@SiNPs@NC foam) (see **Figure 11b**), which could act as a self-standing Si-based anode for high-performance LIBs. The design of the NC foam was based on the conductivity principle, and the MXene-based layer provided the advantage of electrons/ion diffusion while allowing the anode to adapt to large changes in Si volume during lithiation/desalination. The independent MXene@SiNPs@NC foam electrode had a capacity (1658 mAhg^{-1} after 100 cycles at 0.1 °C) and a residual capacity (857 mAhg^{-1} after 500 cycles at 0.5 °C). Moreover, the battery developed entirely using MXene@SiNPs@NC foam //NCM111 exhibited a high gravimetric energy density (433 Wh kg^{-1}). This MXene@SiNPs@NC foam anode demonstrated good electrical properties.

Silicon (Si) is considered one of the candidates that can replace graphite in anodes. Lithium-ion batteries store greater energy and, therefore, improve returns. However, the high mechanical stress caused by its high volumetric variation during charge and discharge cycles, added to its low electrical conductivity, has impeded its wide use. For this reason, silicon-based composites are studied to find out their commercial viability. MXene Ti_3C_2 is a two-dimensional material whose good mechanical resistance and conductivity can contribute to solving the problems of Si anodes. The results revealed that the addition of Ti_3C_2 particles to electrodes could reach 80% and 89% of their theoretical capacity when Ti_3C_2 represents 20% and 40% of the mass of the active electrode material, respectively, compared to the 56% achieved by the pure Si electrode. This improvement is explained by a reduction in

the resistance to charge transfer observed in the EIS results. Finally, the electrode with 20% by weight of Ti_3C_2 (640 mAhg^{-1}) obtained the best specific capacity after 100 charge and discharge cycles than obtained by the pure Si electrode (572 mAhg^{-1}) [67].

Flexible pressure sensors are one of the most important sensors in electronic skin (e-skin), robotics, and medicine. However, sensors are still complex and expensive due to power consumption, unreliable operation, and manufacturing processes. $Ti_3C_2T_X$ is the most studied MXene in the field of pressure sensing, with good mechanical and electrical properties, excellent hydrophilicity, and flexibility. It increases the sensitivity of pressure sensors and the efficiency of the electrode process and continues to use pressure measurements in various areas, such as electrical skin elasticity. The MXene can be used in pressure sensors, which include piezoresistive, capacitive, piezoelectric, triboelectric, and potentiometric switching technologies. Integration of various devices is also possible [68].

5.3.2. MXene promoting beyond lithium battery

The lithium-based battery is undoubtedly the most studied and analyzed battery in scientific literature. However, lithium is not abundant in the earth's crust and will soon suffer the same fate as the overconsumption of fossil fuels, forcing us to look beyond lithium. Fortunately, research on other metal-ion batteries (sodium, potassium, aluminum, magnesium, zinc, etc.) has rapidly increased, and much has been borrowed from research on lithium-ion batteries. Although their theoretical capacity is lower than that of lithium [69], they can reduce the cost of lithium resources by serving as another energy store. The lithium-ion battery has been a leader in the electronics industry and research and development for nearly two decades. Due to concerns about the cost and future availability of lithium, sodium-ion batteries (SIBs) and other new technologies are emerging as candidates for sustainable energy. Research in this technology is increasing, with a focus on developing new cathode and anode materials that can improve cycle stability, operating costs, and energy. 2D materials are promising in many energy-related applications, especially energy storage, due to their ability to transport ions between layers and over large areas, enhanced ion adsorption, and rapid surface redox reactions [70]. Tang et al.'s [70] potassium metal batteries are considered attractive alternatives to lithium-ion batteries. However, uncontrollable dendrite growth of potassium metal anodes limits their practical applications. Functionalization of the potassium anode has been reported to be achieved by encapsulating the metal in a titanium-free, nitrogen-containing MXene/carbon nanotube freestanding scaffold. High and fast electrical conduction in the scaffold helps reduce density and current flow during coating/stripping. Additionally, theoretical calculations and experimental studies confirmed that the "potassium-loving" form of MXene can cause potassium nucleation and add potassium during exposure to stabilize the products. As a result, the produced potassium metal anode exhibits dendrite-free morphology, high Coulomb efficiency, and a long lifetime during the plating/stripping process. Such anodes also improve the electrochemical performance of potassium-sulfur batteries compared to bare metal anodes. The potential of Ti_2N monolayers and their Ti_2NT_2 derivatives (T = O, F, and OH) as

anode materials for lithium-ion and ultra-lithium-ion batteries were investigated by first-principle calculations. The single layer exposed and removed is a very good metal material. The diffusion barriers of the bare Ti_2N monolayer were approximately Li^+ 21.5 meV, Na^+ 14.0 meV, K^+ 7.0 meV, Mg^{2+} 75.9 meV, and Ca^{2+} 38.0 meV. The 2D functional groups of Ti_2NT_2 increased the conduction effect by approximately 1-fold. The calculated capacity of single cations of Ti_2N and Ti_2NT_2 was close to conventional graphite anodes in lithium-ion batteries. In comparison, the Mg^{2+} capacity of Ti_2N and Ti_2NT_2 exceeded 2000 $mAhg^{-1}$ due to the two-electron reaction and multilayer adsorption of Mg^{2+}. A comparison of the electrical properties of Ti_2N and Ti_2C showed that Ti_2N is a better material than Ti_2C due to its sensitivity to various cations [24] (see **Figure 12a**).

The heavy reliance on LIBs has led to growing concerns about the sustainability of lithium and alternative metals and ethical issues in mining. Developing alternative energy storage technologies beyond lithium has become an important part of the world's energy research portfolio [71]. Other technologies, from electric transportation to renewable energy to large-scale energy storage, play an important role in developing energy storage for the future. Considering their chemical and economic benefits, potassium ion batteries (PIBs) are promising and are becoming strong competitors to LIBs and SIBs in many forms. However, many people do not understand the process by which potassium is deposited in materials and how it differs from lithium and sodium, and the material liquid interface chemistry in PIBs is also not fully understood. Therefore, there are still some important problems in the commercialization of PIB technology.

5.4. Supercapacitor

Supercapacitors have attracted significant attention as promising successors to traditional energy storage devices due to several key advantages like higher power density, faster charge-discharge cycles, and greater energy density over batteries and conventional dielectric capacitors [1,22]. There are two main types of supercapacitors based on their working principles: electrochemical double-layer capacitors (EDLC), pseudocapacitors, and hybrid capacitors. EDLCs store energy by the adsorption/desorption of ions on the surface through the electrical double layer, whereas pseudocapacitors store energy through surface redox reactions [4]. The energy density (E) of supercapacitors is governed by the formula $E = CV^2/2$, where C is capacitance and V is voltage. Therefore, enhancing capacitance and voltage window results in higher energy density supercapacitors. Voltage remains relatively constant for a specific electrolyte, so increasing capacitance is crucial for overall capacitor performance improvement [2,22]. As a result, there is significant research interest in enhancing capacitance to improve supercapacitor performance.

MXene exhibits significant potential as an electrode material for batteries and supercapacitors, due to its remarkable electrochemical properties resulting from the presence of transition metal carbide/nitride components and its high electrical conductivity [28]. MXenes typically originate from the MAX phase, which follows the general formula $M_{n+1}AX_n$. Here, M represents an early transition metal, A is a group of 13 or 14 elements, and X consists of C and/or N; n is generally 1–3. MXene

formation occurs through the chemical etching of the A layer within the MAX phase using fluoride ion-containing solutions such as hydrofluoric acid (HF) [11]. Following the etching process, the configuration of MXene may exhibit significant variations, depending on the specific post-treatment method employed. After selectively etching the A layer with HF, the resultant powder manifests a multi-layered MXene structure [72]. In this structure, the atoms of the A layer, predominantly Al or Si, are substituted by terminal groups such as –O, –OH, and/or –F, leading to a phase denoted as $M_{n+1}X_nT_x$. Otherwise, when intercalants like Li^+ ions are used instead of etchants, sonication yields a colloidal phase comprising few-layered or monolayer-exfoliated MXene nanosheets. These exfoliated MXene nanosheets reveal a significantly expanded surface area due to the removal of the A layer spacing. Generally, the use of alkali metal ions as intercalants results in an enlargement of the surface area by at least a factor of two compared to that of the multilayered MXene [33,34,73]. Upon the exfoliation of MXene nanosheets, stacked layers will probably form in MXene films, driven by impromptu attractive interactions such as van der Waals forces and hydrogen bonding [36]. MXene films offer the benefits of flexibility, large conductivity, and surface hydrophilicity, making them favorable for enhanced electrochemical processes. Consequently, free-standing films based on MXene have been widely employed as active materials in supercapacitors and various electrochemical electrodes [37–38,74]. While MXene films possess numerous advantages, their applications are limited due to the lack of regulated film-forming processes [75]. While monolayer MXene nanosheets allow for the optimization of theoretical surface area and electrochemical surface activity, processes primarily involving layer-stacking film formation compromise the intrinsic properties anticipated from monolayers, thus affecting the performance of electrochemical applications [22,76].

Couly et al. proposed a simple approach to fabricate asymmetric micro-supercapacitors using MXene. These micro-supercapacitors are modifiable, free of binder, and current-collector-free. The method involved employing a customized mask and an expandable spray coating technique on a flexible and transparent substrate [77]. The electrode comprised titanium carbide MXene ($Ti_3C_2T_x$) and reduced graphene oxide, both possessing a 2D layered structure that facilitated rapid ion diffusion within the interdigitated electrode framework. This asymmetric micro-supercapacitor operated within a 1 *V* voltage window and retained 97% of its initial capacitance after ten thousand cycles. Furthermore, it demonstrated an energy density of 8.6 mW hcm^{-3} at a power density of 0.2 W cm^{-3}. Moreover, these micro-supercapacitors exhibited remarkable flexibility under mechanical bending. By leveraging the capacity of $Ti_3C_2T_x$—MXene electrodes to operate at negative potentials in aqueous electrolytes, it was demonstrated that employing $Ti_3C_2T_x$ as a negative electrode and reduced graphene oxide as a positive electrode in asymmetric configurations represented a viable approach to enhance both the energy and power densities of micro-supercapacitors.

Rakhi et al. [78] developed 2D Ti_2CT_x MXene nanosheets by selectively etching the Al layer from the Ti_2AlC MAX phase, utilizing HF. The hexagonal symmetry of the parent Ti_2AlC MAX phase was preserved in the MXene sheets. An extensive investigation was conducted to evaluate the influence of various post-etch

annealing atmospheres, including argon (Ar), nitrogen (N$_2$), a combination of nitrogen and hydrogen (N$_2$/H$_2$), and air, on both the structure and electrochemical characteristics of the MXene nanosheets. It was found that the MXene sheets displayed changes in structure, morphology, and electrochemical behavior following annealing in air compared to the HF-treated MAX phase. In contrast, samples subjected to annealing in Ar, N$_2$, and N$_2$/H$_2$ atmospheres maintained their initial morphology. A substantial enhancement was observed in the supercapacitor performance of the annealed samples, particularly in those annealed in Ar, N$_2$, and N$_2$/H$_2$ atmospheres. In a symmetric two-electrode setup, the MXene sample annealed in an N$_2$/H$_2$ atmosphere exhibited superior capacitive performance, boasting a specific capacitance of 51 Fg^{-1} at 1 Ag^{-1} and an impressive rate performance of 86%. This notable enhancement in electrochemical performance post-annealing was attributed to several factors, including the increased carbon content, decreased fluorine content on the surface, and the preservation of the original two-dimensional layered morphology, ensuring optimal access of the aqueous electrolyte to the electrodes.

Wen et al. [79] introduced a novel electrode material for supercapacitors, nitrogen-doped two-dimensional MXene (N-Ti$_3$C$_2$T$_x$), through annealing of Ti$_3$C$_2$T$_x$ in ammonia post-etching. Through precise control of annealing temperatures within the range of 200 °C to 700 °C, the concentrations of nitrogen in N-Ti$_3$C$_2$T$_x$ materials were made ranging from 1.7% to 20.7%. The incorporation of nitrogen as a heteroatom into the Ti$_3$C$_2$T$_x$ structure led to an expansion of the c-lattice parameter in MXene sheets, from 1.92 nm in Ti$_3$C$_2$T$_x$ to 2.46 nm in N-doped counterparts after treatment with ammonia at 200 °C. The resultant doped MXene materials exhibited significantly enhanced electrochemical capacitance of 192 F/g in 1 M H$_2$SO$_4$ and 82 F/g in 1 M MgSO$_4$ electrolyte, under optimized conditions. These values represented a substantial rise in the capacitances, as observed for undoped Ti$_3$C$_2$T$_x$ materials, which recorded 34 F/g in 1 M H$_2$SO$_4$ and 52 F/g in 1 M MgSO$_4$ (see **Figure 12b**).
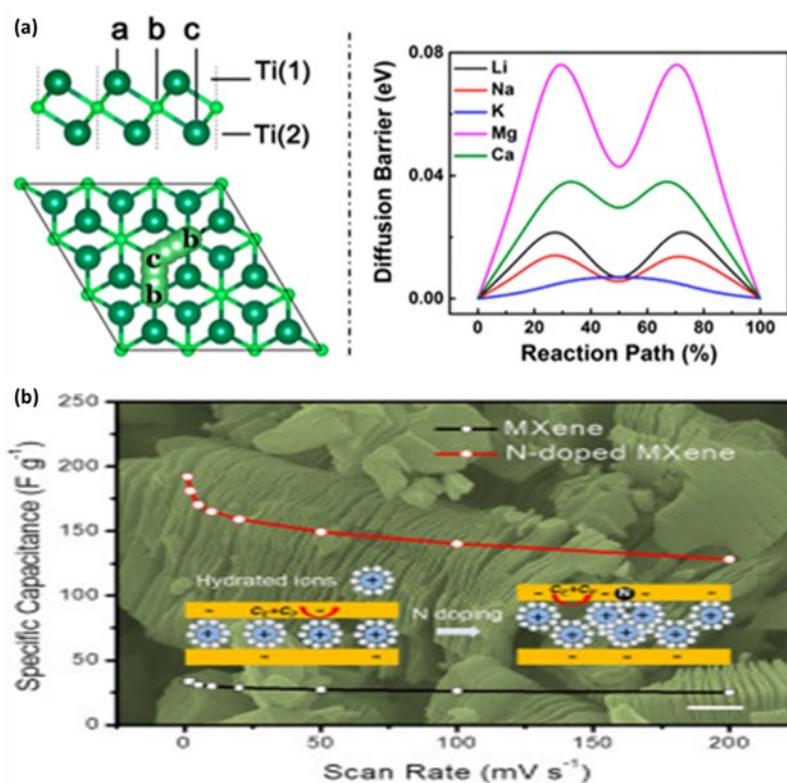
Figure 12. (a) First calculations of Ti_2N and Ti_2NT_2 (T=O, F, OH) monolayers as anode materials for lithium-ion batteries and other batteries [24]; **(b)** nitrogen-doped $Ti_3C_2T_x$ MXene electrodes for high-performance supercapacitors [79].

5.5. Biomedical applications

Levitt et al. [80] fabricated free-standing $Ti_3C_2T_x$ MXene/carbon nanofiber electrodes by electrospinning to combine $Ti_3C_2T_x$ MXene flakes with polyacrylonitrile (PAN), followed by carbonization. Through this approach, delaminated MXene flakes could be incorporated within carbon nanofibers, resulting in fiber mats that could be employed as electrodes. Notably, these composite electrodes exhibited superior sturdiness compared to their coated counterparts. In the spinning dope, MXene flakes were introduced into PAN solutions at a weight ratio of 2:1, resulting in fiber mats containing MXene up to 35 wt%. The resulting composite electrodes demonstrated an impressive areal capacitance of up to 205 mF cm^{-2} at 50 mV s^{-1}, nearly three times higher than that of pure carbonized PAN nanofibers, which registered at 70 mF cm^{-2} under the same conditions. Furthermore, in comparison to electrospun nanofibers spray-coated with $Ti_3C_2T_x$, these composite fibers exhibited a twofold increase in areal capacitance at 10 mV s^{-1} (refer to **Figure 13a**). This versatile technique holds promise beyond energy storage applications, as it can be extended to generate MXene composite fibers using a variety of polymers. Such applications may include filtration, adsorption, and electrocatalysis, where fibers with high aspect ratios, accessible surface areas, and porosity are highly desirable.

5.6. MXene as gas sensors

Kim et al. [81] introduced chemical sensors with exceptional gas-sensing

characteristics through the synthesis of $Ti_3C_2T_x$ (see **Figure 13b**). These sensors exhibited remarkable selectivity towards hydrogen-bonding gases compared to acidic gases. Also, an empirical Limit of Detection (LOD) of 50 ppb was achieved and a theoretical LOD reaching the sub-ppb level for Volatile Organic Compounds (VOC), making the lowest detection limits among gas sensors utilizing 2D materials and functioning at room temperature without any pretreatment. Furthermore, the signal-to-noise ratio (SNR) of $Ti_3C_2T_x$ sensors surpassed that of all other 2D materials by up to two orders of magnitude. The remarkable sensitivity of $Ti_3C_2T_x$ sensors could be attributed to both the metallic conductivity of the core channels and the robust adsorption energy of the surface functional groups (**Figure 13b**) [82].
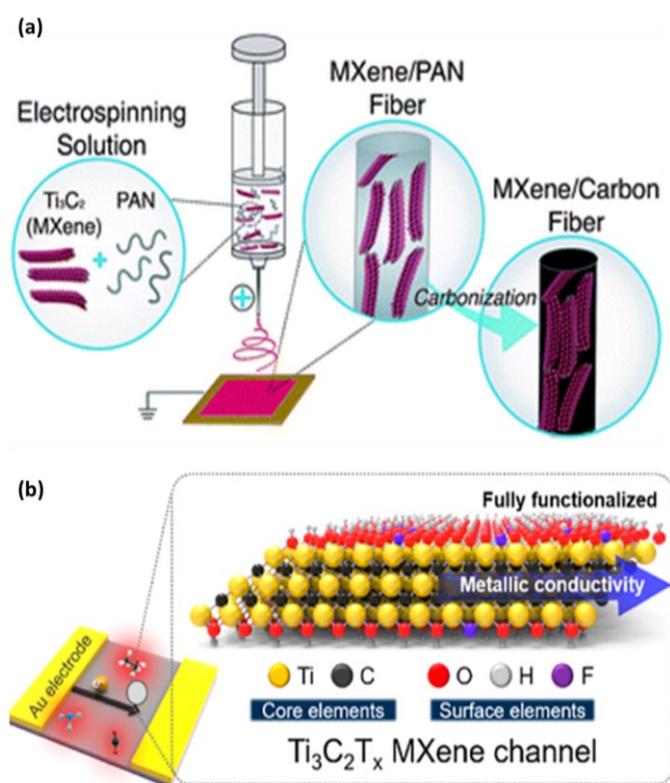

Figure 13. (a) Electrospun MXene/carbon nanofibers as supercapacitor electrodes [81]; **(b)**Schematic representation of $Ti_3C_2T_x$ films [82].

5.7. Sensors in biomedical applications

The distinctive 2D layered structure and remarkable array of physical and chemical attributes exhibited by MXenes, such as hydrophilic nature, biocompatibility, adeptness in light-to-heat conversion, and mechanical resilience, make them promising candidates across diverse biomedical domains. These applications encompass sensor technologies, bioimaging modalities, tissue engineering approaches, and advanced drug delivery systems.

Biosensors

Upon their discovery, MXenes swiftly ascended as a profoundly promising category of 2D materials. Their notable characteristics, including a substantial specific surface area, elevated conductivity, near-infrared absorption, and ease of functionalization, make them exceptionally well-suited for biomedical and

environmental applications (**Tables 1** and **2**) [83]. In in-vitro experiments, MXenes exhibit toxicity against bacterial and animal cells, primarily due to mechanisms such as oxidative stress and the mechanical damage inflicted on cell membranes by the sharp edges of the nanosheets (**Figure 14a**).
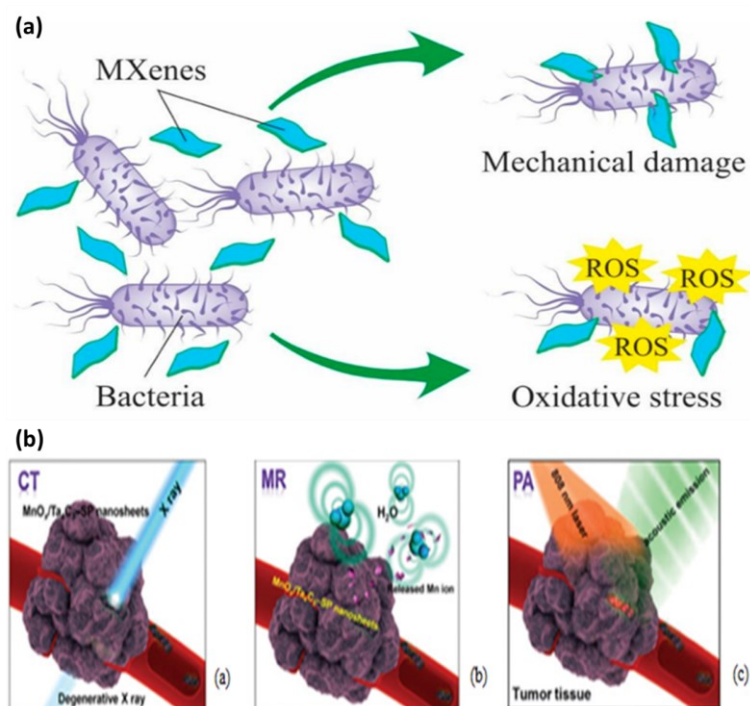

Figure 14. (a) Schematic representation of cytotoxic effects of MXene on bacterial cells [83]; **(b)** Schematic representation of **(a)** In vivo computed tomography Imaging of the Ta_4C_3 MXene composite **(b)** Disintegration of MnOx components from MnOx/Ta_4C_3 under a specific tumor microenvironment for contrast-enhanced T1-weighted magnetic resonance imaging **(c)** In vivo photoacoustic imaging [84].

Table 1. Biosensors for medicinal use [83].

Sensor Composition	Detectable Analyte	Sensor Type	Sensor Efficiency
MXene-Ti_3C_2	Hemoglobin	Electrochemical biosensors	detection limit of 20 nM
MXene-Ti_3C_2	Hemoglobin	Electrochemical biosensor	linear range of 0.5–11,800 μM, detection limit of 0.12 μM
GOx/Au/$Ti_3C_2T_x$-MXene/Nafion/GCE	Glucose	Electrochemical biosensor (amperometric)	detection limit of 5.9 μM
Ti_3C_2-MXene functionalized with aminosilane	Carcinoembryonic antigen (CEA)	Electrochemical biosensor	linear detection range of 0.0001–2000 ng mL^{-1} with sensitivity of 37.9 μA $ng^{-1}mL\ cm^{-2}$ per decade
Ti_3C_2	Human papillomavirus (HPV)	Optical biosensor	detection limit of 100 pM
Ti_3C_2Tx MXene and phosphomolybdic acid embedded with polypyrrole	Osteopontin	Aptamer biosensor	0.98 μg/L
Ti_3C_2Tx/PtNP modified GCE	Ascorbic acid, dopamine, uric acid, acetaminophen	Electrochemical biosensor	nM level
OH-terminated Ti_3C_2	Label-free single-nucleotide in human urine	Electrochemiluminescence biosensor	Detection limit of 5 nM

Table 1. (*Continued*).

Sensor Composition	Detectable Analyte	Sensor Type	Sensor Efficiency
Ti_3C_2Tx/Prussian blue	Glucose and lactate in sweat	Electrochemical biosensor (amperometric)	Sensitivities of 35.3 μA $mm^{-1}cm^{-2}$ for glucose and 11.4 μA $mm^{-1}cm^{-2}$ for lactate
MXene-Ti_3C_2Tx incorporated with a dialysis microfluidic chip	Urea, uric acid, and creatinine	Electrochemical biosensor	
MXene-Ti_3C_2Tx modified screen-printed electrode	Acetaminophen (ACOP), isoniazid (INZ)	Electrochemical biosensor	Linear ranges from 0.25 to 2000 μM for ACOP and 0.1–4.6 mM for INZ. The detection limits of ACOP and INZ were 0.048 μM and 0.064 mM
Ti_3C_2Tx/ZIF-8	HIV-1 protein	Electrochemical biosensor	detection limit 0.3 fM
Au/Ti_3C_2T/HB5	HER2-positive cancer cells	Electrochemical cytosensor	linear range of 10^2–10^6 cells/mL, detection limit of 47 cells/mL
Chit/ChOx/Ti_3C_2Tx	Cholesterol	Electrochemical biosensor	concentration of cholesterol ranging from 0.3 to 4.5 nM, detection limit of 0.11 nM, sensitivity of 132.66 μA $nM^{-1}cm^{-2}$
Ti_3C_2Tx MXene/LBG/PDMS	Cortisol	Electrochemical impedimetric immunosensor	linearity 0.01–100 nM, detection limit 88 pM
PEI-Ru@Ti_3C_2@AuNPs	SARS-CoV-2 RdRp gene	Electrochemiluminescent biosensor	Detection limit of 12.8 aM
ZnO/Ti_3C_2	Glucose	Electrochemical enzymatic biosensor	Sensitivity 29 μA $mM^{-1}cm^{-2}$, limit of detection $\approx$ 17 μM, linear detection range 0.05–0.7 mM)

Table 2. Biosensors for environmental use [83].

Sensor Composition	Detectable Analyte	Sensor Type	Sensor Efficiency
$Mo_2Ti_2AlC_3$/MWCNT	Bisphenol A	Electrochemical biosensor (amperometric)	0.01–8.50 μM
MXene-Ti_3C_2	Tyrosinase	Electrochemical biosensor	linear range from 0.05 to 15.5 μM L^{-1}, detection limit of 12 nM L^{-1}
MXene-Ti_3C_2	Ag^+ and Mn^{2+}	Optical sensors	Range of 0.1–40 μM for Ag^+, detection limits of 9.7 nM; 0.5–60 μM for Mn^{2+}ions,
Ti_3C_2Tx (MXene)-modified glassy carbon electrode	BrO_3^-	Electrochemical biosensor	linear response from 50 nM to 5 μM, detection limit of 41 nM
Hydroxyl terminated alk-Ti_3C_2 modified GCE	Cd(II), Pb(II), Cu(II) and Hg(II)	Electrochemical biosensor	Detection limit of 0.098, 0.041, 0.032 and 0.130 μM for Cd(II), Pb(II), Cu(II) and Hg(II), respectively
AChE-Chit/Ti_3C_2-MXene/Au NPs/MnO_2/Mn_3O_4/GCE	Organophosphorus pesticides	Electrochemical biosensor	concentration range (10^{-12}–10^{-6}M), limit of detection (1.34×10^{-13}M)
AChE/CS-$Ti_3C_2T_x$/GCE	Organophosphorous pesticides (malathion)	Electrochemical biosensor	concentration range of 10^{-14}–10^{-8}M, limit of detection 0.3×10^{-14}M
AChE/Ag@$Ti_3C_2T_x$	Organophosphorous pesticides (malathion)	Electrochemical biosensor	concentration range of 10^{-14}–10^{-8} M
$Ti_3C_2T_x$	carbamate pesticides (methiocarb and diethofencarb)	Electrochemical biosensor	detection limits were 0.19 μg mL^{-1} and 0.46 μg mL^{-1} for methiocarb and diethofencarb respectively
CdS/MXene-NH_2/Zn_5nO_3	Cd^{2+}, perfluorohexane	Photoelectrochemical biosensor	linear range of 0.008–100 nM, detection limit of 4.21 pM
$MnMoO_4$-MXene-GCE	Hydroquinone, catechol	electrochemical biosensor	linear response from 5 nM to 65 nM, detection limit of 0.26 nM for Hydroquinone and 0.30 nM for catechol

The interest in early detection of cancer has grown in the context of bioimaging and biosensing, owing to their capacity to unveil intricate cellular processes and a diverse array of diagnostic indicators. Ti_3C_2 is the most extensively researched MXene nanostructure in applications related to bioimaging and biosensing, while Ta_4C_3 MXene is commonly employed for multimodal imaging. The presence of tantalum (Ta) in the Ta_4C_3 MXene, characterized by a high atomic number and a notable X-ray attenuation coefficient, enables its utilization in CT imaging without requiring supplementary contrast agents. This streamlines the setting up of multimodal imaging. Regarding biosensing, platforms utilizing MXenes have been developed for various techniques, including electrochemistry, fluorescence, surface plasmon resonance, surface-enhanced Raman scattering, and colorimetric and chemiluminescence-based biosensing [84] (see **Figure 14b**).

Surface modification and functionalization are pivotal in augmenting the characteristics of materials based on MXene. Following surface modification, MXene-based materials have been propelled into the spotlight and have found widespread application in various fields, such as biomedicine, energy, and the environment. Specifically, this includes biosensing, drug delivery systems, bioimaging, photothermal therapy, antibacterial agents, and theragnostic nanoplatforms within the realm of biomedical applications [85].

5.8. Flexible pressure sensor

MXenes have found application in different sensing scenarios because of their adjustable surface functionalities. Sensors based on MXenes have proven effective in detecting a range of pollutants, exhibiting a lower detection limit and impressive selectivity/sensitivity [85,86]. The domains of electronic skin, human-machine interaction, and health monitoring demand pressure sensors that are both flexible and highly sensitive. However, most microstructure designs employed for creating pressure sensors with high performance involve intricate preparation processes. Yin et al. [87] obtained a 3D porous structure of MXene/polyaniline (PANI) foam through the application of a steam-induced foaming method. Utilizing this structure, a flexible piezoresistive sensor was manufactured. It demonstrated remarkable characteristics, including high sensitivity (690.91 kPa^{-1} quick response and recovery time of 106/95 ms, and excellent fatigue resistance (10,000 cycles). The pressure sensor, derived from MXene/PANI foam, could rapidly perceive subtle pressure changes. It was found suitable for applications in human activity and supervision of health [86,87].

As composite materials find extensive use in aeronautic structures, research on composite material repair methods is becoming increasingly comprehensive. However, owing to the unique nature of the composite materials, the visual efficacy of repairs and the service condition of the composite repaired structure is challenging, necessitating highly sensitive piezoresistive strain sensors. Wang et al. [88] introduced an innovative MXene film sensor technology capable of real-time and in-situ health monitoring of composite structures. The proposed method enabled the creation of MXene thin films with exceptional properties. MXene sensors were produced and organized into arrays and integrated into the composite repair structure to monitor strain across various points. The piezoresistive reaction of the MXene

sensor was acquired, and the primary operational mechanism was elucidated. The strategic arrangement of MXene sensors in the repaired structure enhanced the monitoring process, offering a more thorough understanding of the failure mechanism. This monitoring approach, utilizing MXene sensors, can be used for investigating the health status of composite repair structures under both tensile and compression conditions [88] (see **Figure 15**).
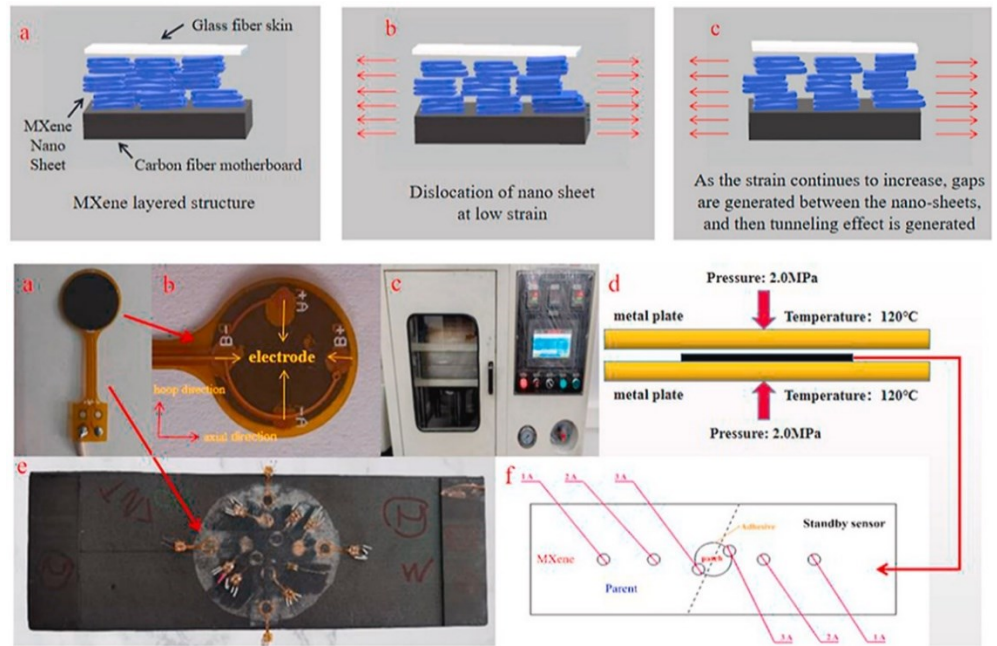

Figure 15. Monitoring of repaired composite structure [88].
Sen mechanism of MXene sensor and sensor array arrangement of composite material repair structure.

Despite possessing notable properties such as a large surface area, biocompatibility, metallic conductivity, hydrophilicity and tunable size, the application of MXene in biomedical settings is constrained by its limited stability in physiological environments, absence of sustained and controlled drug release, and low biodegradability. These challenges have prompted consideration for the adoption of MXene/polymer nanocomposites. The presence of functional groups on the MXene surface allows for polymer functionalization. Hence, these MXene nanocomposites functionalized with polymers showcase notable features such as high photothermal conversion efficiency, selectivity, responsiveness to stimuli, electron sensitivity, enhanced antibacterial properties, and more. These characteristics make them suitable for use in biomedical applications, including photothermal therapy, drug delivery, diagnostic imaging, biosensing, bone regeneration, and antibacterial activities [89] (see **Figure 16**).
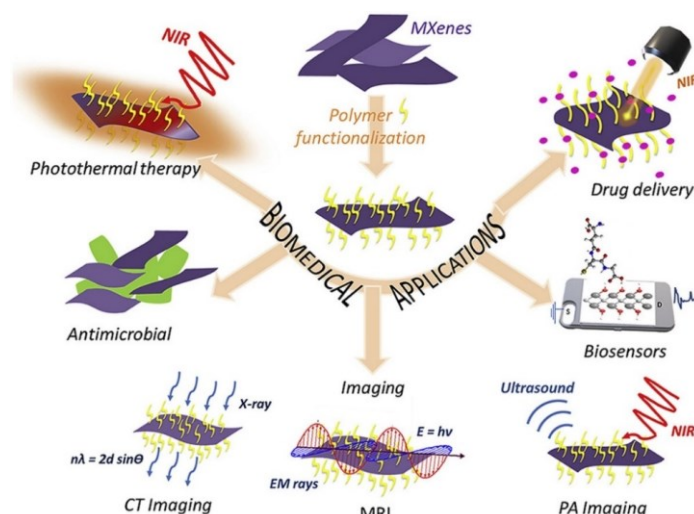
Figure 16. MXene-Polymer composites in biomedical applications [89].

5.9. Drug delivery system

The healing of chronic wounds is a fundamental and significant concern in medical and healthcare domains, and in recent times, hydrogel systems have emerged as promising carriers for drug delivery in the context of wound management, which is responsive to stimuli. Yang et al. [90] introduced a hydrogel system based on 2D MXene, designed for effective drug delivery with photo- and magnetic-responsive capabilities, specifically tailored for the treatment of deep chronic wounds. The smart and responsive drug delivery system using MXene consisted of magnetic colloids enveloped by MXene and dual-network hydrogels made from poly (N-isopropyl acrylamide) and alginate. It exhibited versatile responsiveness and precise drug release mechanisms, effectively mitigating the toxic side effects of drugs and enhancing the wound healing process. The real-world efficacy of the MXene-based hydrogel drug delivery system was validated through its application in treating full-thickness cutaneous wounds and subcutaneous infected wounds in a rat model, highlighting its substantial potential in clinical wound healing management and other relevant biomedical domains.

5.10. MXene in cancer treatment

Typical approaches to cancer treatment encompass surgical procedures, chemotherapy, and radiotherapy involving the use of anti-cancer medications. Recently, MXenes have generated considerable attention for their potential use as drug carriers. This is attributed to their planar structure, abundant surface functional groups, biocompatibility, and negatively charged surface. Even though nanosized Ti_3C_2, the pioneering MXene for drug delivery vehicles, exhibits an enhanced permeability and retention effect that allows it to accumulate at the tumor site, surface modification is essential. This is because it tends to restack under physiological conditions. The tumor microenvironment, which typically has a lower pH compared to normal tissues, offers an opportunity for controlled drug release, as the presence of H^+ ions can disrupt the electrostatic interaction between the drug and MXene. Additionally, controlled drug release can be achieved through near-infrared radiation stimulation [91].

Micro- and nanosystems incorporating MXene can be utilized for precise administration of anticancer drugs or therapeutic agents, offering the benefits of minimal toxicity and excellent biocompatibility. Confirming the effective uptake of therapeutic chemicals from the bloodstream to the intended site presents a significant challenge in systemic disposition. The vascular endothelial cell, serving as a barrier between organs and blood, emerges as a crucial focal point in this regard. By incorporating MXene into composites and subsequently functionalizing or modifying them with appropriate functional groups or agents, their loading capacity, biocompatibility, and bioavailability can be enhanced [92]. MXene-based micro- and nanosystems, following surface functionalization or modification with bioactive or biocompatible agents, have been employed for targeted delivery of anticancer drugs or therapeutic agents in cancer therapy (**Figure 17**) [92].
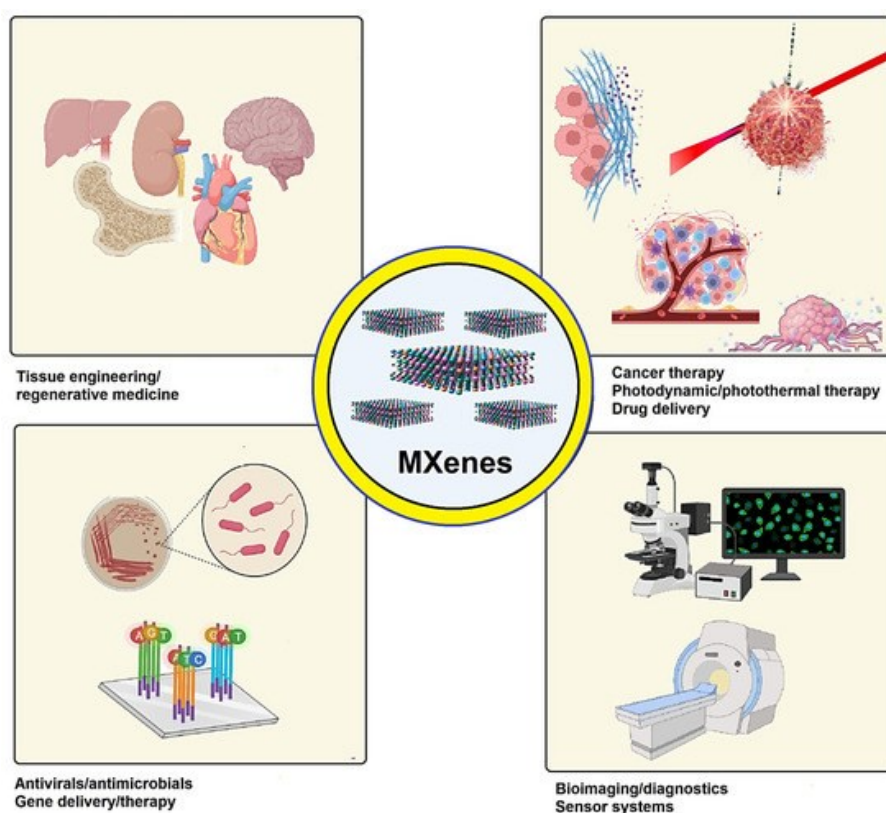

Figure 17. MXene with potential biomedical applications [92].

Liu et al. [93] described the creation of a drug delivery platform for the efficient loading of the chemotherapeutic doxorubicin (DOX) (see **Figure 18**). This platform exhibited dual drug release modes, responding to both near-infrared laser stimulation and variations in pH. Due to the surface modification involving thiol polyethene glycol aldehyde chains (SH-PEG-CHO) linked to the MXene through gold nanoparticles, the MXene@Au-PEG-DOX system exhibited favorable photothermal stability, biocompatibility, and tissue compatibility. Furthermore, using the effective photothermal conversion capabilities of both gold particles and MXene, it demonstrated a synergistic approach to combine photothermal ablation with chemotherapy to treat tumors. The enhancement of MXene through surface modification involving Au and PEG served not only to enhance the photothermal

stability of the drug delivery system and the biocompatibility of the nanocomposites but also to regulate drug release through the formation of Schiff base bonds. Consequently, this, in turn, led to improved targeted therapeutic effects.
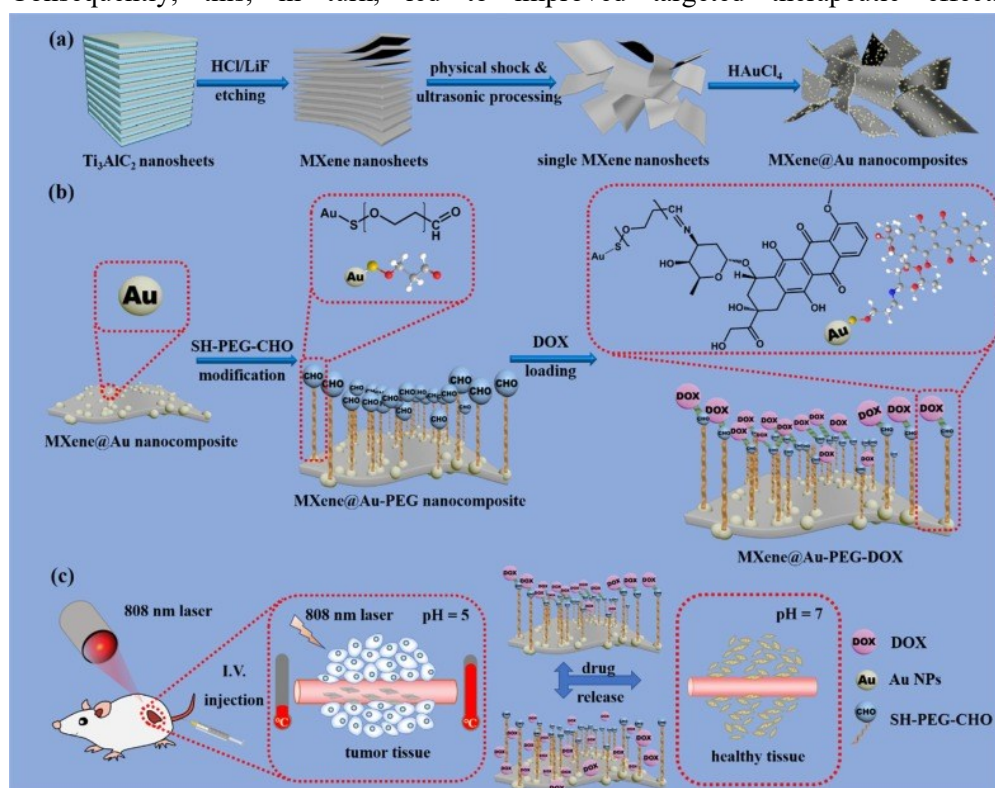

Figure 18. (a) Illustrative diagram of fabrication of MXene and MXene@Au nanosheets; **(b)** modification of MXene@Au surface using thiol polyethylene glycol aldehyde chains (SH-PEG-CHO), and DOX loading; **(c)** illustrative representation of MXene-based drug delivery system for near-infrared laser-triggered and pH-responsive drug release in tumor tissue [93].

A drug carrier with targeting capabilities for folate receptors was developed by Liu et al. [93], leveraging the plentiful surface functional groups and outstanding biocompatibility of MXenes. The drug carrier exhibited a drug-loading capacity of up to 69.9%, along with an extended drug release duration of up to 48 h. The findings indicated a substantial release of DOX in a pH 4.5 PBS solution. In comparison to the free drug, MXenes-FA-SP@DOX demonstrated increased cell inhibition and prolonged drug efficacy at lower concentrations (below 10 μg mg^{-1}). This drug delivery system can be used for the treatment of malignant tumors. Dong et al. [94] synthesized drug-loaded MXene/agarose hydrogel (MXene@Hydrogel). Initially, superior photothermal conversion efficiency and stability were achieved by preparing two-dimensional MXene nanosheets. Subsequently, these MXene nanosheets, along with the therapeutic drug, were integrated into a low-melting-point agarose hydrogel network to form the drug-loaded MXene/agarose hydrogel (MXene@Hydrogel). Incorporating a low concentration of MXene (20 ppm) facilitated rapid heating of the MXene@Hydrogel to 60 °C under near-infrared (NIR) irradiation, prompting its melting and subsequent release of encapsulated drugs. Control over drug release kinetics and on/off functionality could be easily

modulated by adjusting agarose concentration, MXene concentration, light intensity, and exposure duration. Moreover, doxorubicin, an anticancer drug, maintained its efficacy upon release from the MXene@Hydrogel network under NIR irradiation. With its outstanding biocompatibility, this NIR-responsive MXene@Hydrogel represents a promising strategy for developing a smart hydrogel-based drug delivery system tailored for localized cancer therapy.

A nanoparticle system (MXene-TK-DOX@PDA) sensitive to reactive oxygen species (ROS) was engineered for efficient drug delivery in chemotherapy and applications in antibacterial therapy by Zhang et al. [95] (See **Figure 19**). The surface of (3-aminopropyl) triethoxysilane (APTES)-functionalized MXene served as a platform for conjugating DOX via a ROS-cleavable diacetyl thioketal (TK) linkage. Following this, the MXene nanosheets were coated with pH-responsive polydopamine (PDA) to serve as a gatekeeper. This incorporation of PDA enhanced the biocompatibility and stability of the MXene-TK-DOX@PDA nanoparticles. The ultrathin planar structure of MXene-TK-DOX@PDA nanoparticles, with a compact lateral size of around 180 nm, showcased exceptional photothermal conversion efficiency, superior stability in photothermal applications, and a notable extinction coefficient of 23.3 $Lg^{-1}cm^{-1}$ at 808 nm. The synthesized nanoparticles demonstrated effective release of DOX, responsive to both ROS and pH, attributed to the cleavage of the thioketal linker in MXene-TK-DOX@PDA. Furthermore, the MXene-TK-DOX@PDA nanoparticles exhibited potent antibacterial effects against both Gram-negative *Escherichia coli* (*E. coli*) and gram-positive *Bacillus subtilis* (*B. subtilis*) within a 5-hour timeframe.
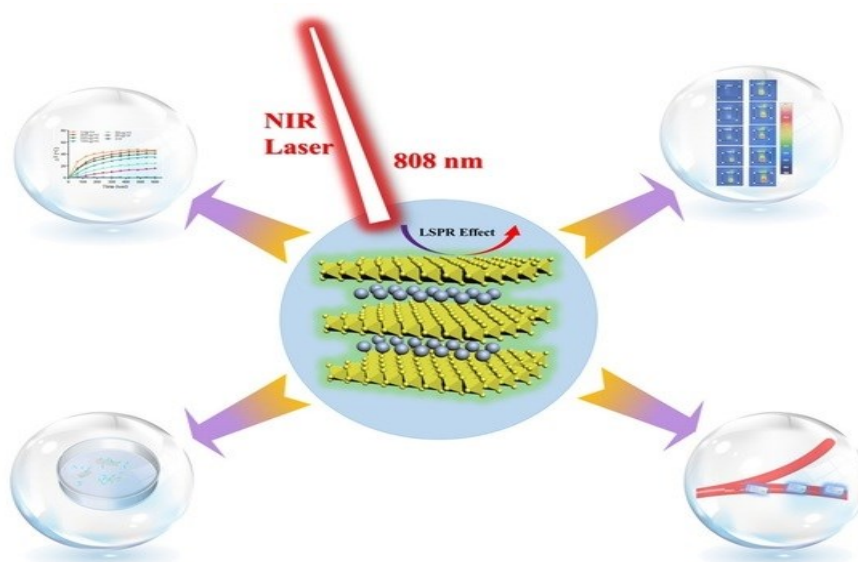

Figure 19. MXene-based nanoparticles as drug delivery carriers [95].

Using a layer-by-layer approach, a drug delivery system with pH/near-infrared responsiveness was created by Wu et al. [96]. This system is comprised of hollow hydroxyapatite (HAP), chitosan (CS)/hyaluronic acid (HA) multilayers, gold nanorods (AuNRs), and MXene. Multilayers of chitosan/hyaluronic acid were applied to the hollow hydroxyapatite (HAP) surface to mitigate the abrupt release of DOX during the initial delivery phase. Integration of MXenes and gold nanorods

(AuNRs) into the hybrid matrix notably enhanced the photothermal conversion efficiency of the microcapsules. The exceptional pH-/NIR-responsive drug delivery properties of HAP/CS/HA/MXene/AuNRs microcapsules were demonstrated through the disruption of electrostatic forces among chitosan/hyaluronic acid multilayers, the dissolution of HAP under acidic conditions, and the synergistically enhanced photothermal effect between MXene and AuNRs.

Liu et al. [97] developed a novel catalyst heterostructure (MXene/CoNWs) activated by NIR radiation, comprising 2D MXene and 1D cobalt nanowires (CoNWs), for combating bacteria without the use of drugs (see **Figure 20**). The incorporated CoNWs swiftly captured photogenerated electrons from Ti_3C_2 MXene nanosheets, thus mitigating the recombination of electron-hole pairs and enhancing carrier transfer under 808 nm NIR illumination, leading to increased reactive oxygen species (ROS) production. Moreover, the 2D/1D heterostructure exhibited a significantly amplified photothermal effect due to synergistic interactions between plasmonic CoNWs and the MXene semiconductor. Coatings of this heterostructure on orthopaedic implants demonstrated antibacterial efficacy exceeding 90% against both Gram-positive and Gram-negative bacteria within a mere 20-minute exposure period. Additionally, in vitro assessments indicated acceptable cytocompatibility of MXene/CoNWs heterojunctions.
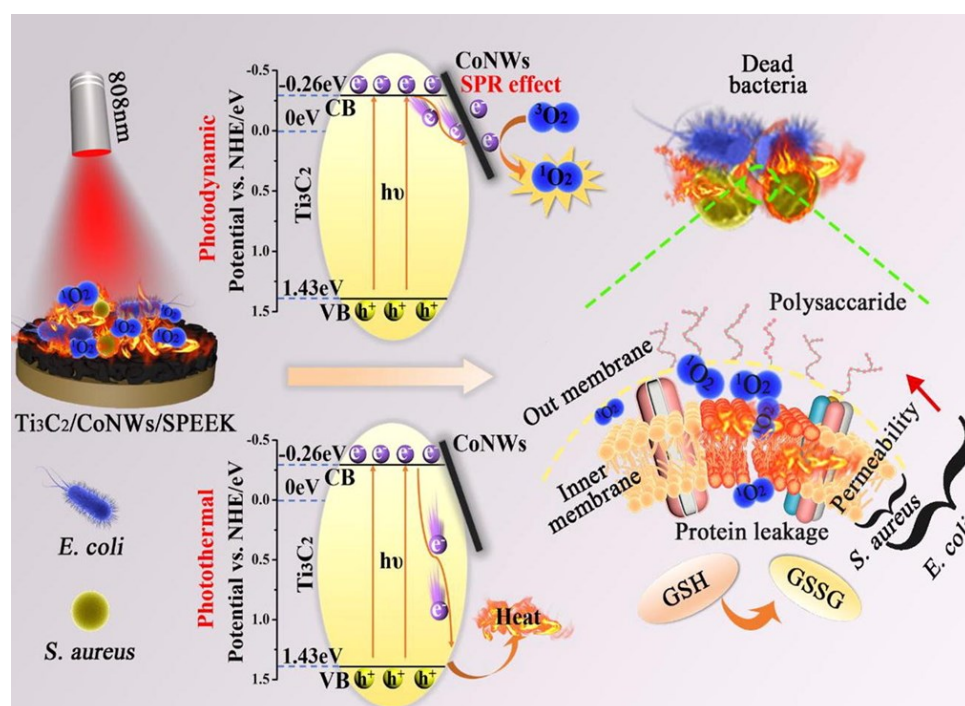

Figure 20. Schematic representation of MXene/CoWNs activation and action on bacteria [97].

5.11. Recent advanced progress in biomedical applications of MXenes

Owing to the captivating physicochemical attributes of MXenes, these materials and their blends have been engineered for diverse biomedical applications. $Ti_3C_2T_x$ was the first MXene to be identified, and it soon emerged as the most extensively researched MXenes. It demonstrated outstanding catalytic characteristics in the field

of photocatalytic Hydrogen Evolution reaction. Nevertheless, the characteristics of $Ti_3C_2T_x$ were significantly influenced by its surface functional groups and associated materials. In particular, $Ti_3C_2T_x$ terminated with oxygen displayed the most optimal catalytic activity. Its efficacy could also be enhanced by combining it with other photoactive materials like TiO_2, ZnO, MoS_2, WS_2, CdS, and graphitic carbon nitride. These composite materials not only enhanced light absorption but also improved charge separation and active sites, thereby enhancing the overall performance of $Ti_3C_2T_x$ under UV-visible light irradiation [98] (See **Figure 21**). Koyappayil et al. [99] modified $Ti_3C_2T_x$ MXene nanosheets by incorporating *β*-hydroxybutyrate dehydrogenase to create a biosensor for amperometric detection of *β*-hydroxybutyrate. MXene demonstrated its excellence as an immobilization matrix, exhibiting strong compatibility with the enzyme *β*-hydroxybutyrate dehydrogenase. The biosensor utilizing MXene, working optimally at a potential of −0.35 V (vs. Ag/AgCl), exhibited a broad linear detection range (0.36 to 17.9 mM), a sensitivity of 0.480 $\mu A\ mM^{-1}\ cm^{-2}$, and a low detection limit (45 μM). Successful application of this biosensor was demonstrated in accurately determining *β*-hydroxybutyrate levels in real serum samples, even when spiked with additional compounds.
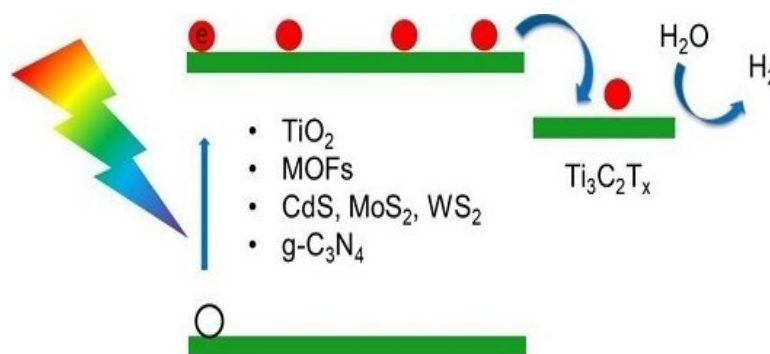

Figure 21. Titanium Carbide MXene in hydrogen production [98].

5.12. Cytocompatibility and cytotoxicity evaluations of MXenes

In contemporary biomedical research, MXene materials are increasingly employed. Zhang et al. [100] conducted experiments to assess the osteogenic potential of $Ti_3C_2T_x$ films, crucial for bone tissue engineering. Results from cellular studies revealed strong compatibility with cells and a propensity to stimulate osteogenic differentiation in vitro. Furthermore, the implantation of MXene films into rat subcutaneous and calvarial defect sites showcased remarkable biocompatibility, osteoinductive properties, and the ability to facilitate in vivo bone regeneration. Examining the potential risks associated with $Ti_3C_2T_x$ MXene exposure to the circulatory system, Huang et al. [101] investigated its cytocompatibility with red blood cells (RBCs) and human umbilical vein endothelial cells (HUVECs). Results indicated excellent compatibility even at high concentrations, with minimal hemolysis observed. Even at a high concentration of 200 μg/mL, $Ti_3C_2T_x$ induced minimal hemolysis at 0.8%, whereas GO at the same treatment concentration resulted in a considerably higher hemolysis rate of 50.8%. The structures of RBCs were left undisturbed. The presence of fully covered surface-terminating –O and –OH groups in $Ti_3C_2T_x$ resulted in a highly hydrophilic surface, impeding its influx

into the inherently hydrophobic interior of the cell membrane (**Figure 22**). The remarkable compatibility of $Ti_3C_2T_x$ nanosheets with cell membranes and their minimal capacity to induce excessive reactive oxygen species (ROS) generation make them compatible with HUVECs.
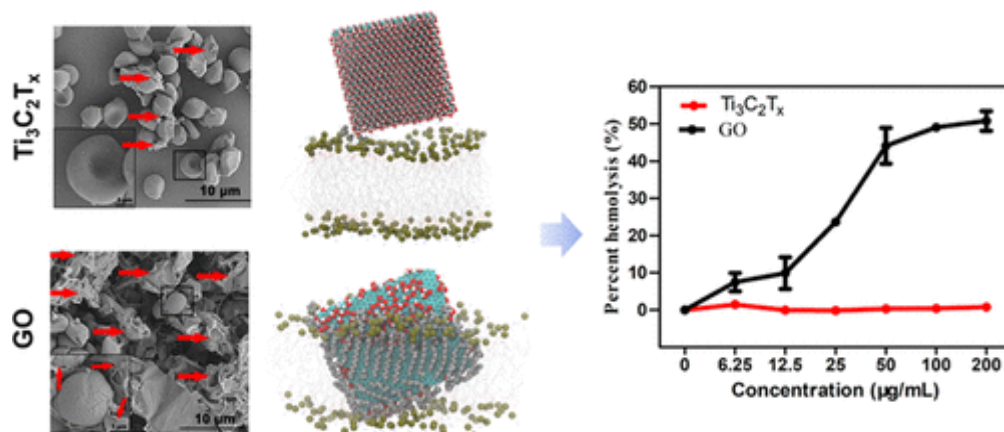

Figure 22. Cytocompatibility of $Ti_3C_2T_x$ MXene with red blood cells and human umbilical vein endothelial cells and the underlying mechanisms [101].

In the realm of flexible electronics and biomedical devices, MXene fibers hold promise due to their superior conductivity. Usman et al. [102] investigated the incorporation of silk fibroin biopolymer into MXene formulations to enhance fiber properties. The addition of silk fibroin led to improved durability, with fibres enduring up to 1 hour of high-frequency sonication. Also, fibers containing approximately 5 wt% silk fibroin demonstrated intriguing characteristics, such as high conductivity (approximately 3700 S cm^{-1}), elevated volumetric capacitance (approximately 910 F cm^{-3}), and non-cytotoxicity towards THP^{-1} monocytic cells. For the development of bioimaging tools, Neubertova et al. [103] suggested covalent functionalization of Ti_3C_2T flakes using the chelating agent diethylenetriaminepentaacetic acid (DTPA), followed by complexation with Gd^{3+} ions. This established functionalization technique endowed the inherently diamagnetic Ti_3C_2T flakes with a paramagnetic response, facilitating their utilization in T1-weighted magnetic resonance (MR) imaging. Additionally, a noticeable relationship between magnetic relaxation time and flake concentration was observed, enabling the estimation of the distribution of flakes in space. The covalent decoration approach applied to MXene resulted in safeguarding its surface against oxidation in phosphate buffered saline and blood serum while enhancing cytocompatibility simultaneously. Furthermore, the chelation of Gd^{3+} ions demonstrated superior prevention of leakage compared to electrostatic chemisorption. A high photothermal conversion efficiency of MXene-Gd was demonstrated, suggesting potential applications in photothermal therapy.

Yang et al. [104] highlighted the emergence of phototherapy as a promising strategy for combating bacterial infections without the associated risk of antibiotic resistance. However, the presence of endogenous antioxidative glutathione (GSH) in bacteria poses a challenge, as it hampers the desired antibacterial effects of externally generated reactive oxygen species (ROS) during phototherapy. A quad-

channel synergistic antibacterial nanoplatform composed of Ti_3C_2 MXene/MoS_2 (MM) 2D bio-heterojunctions (2D bio-HJs) was fabricated. This platform exhibited photothermal, photodynamic, peroxidase-like (POD-like), and glutathione oxidase-like properties. Upon exposure to NIR laser, the 2D bio-HJs induced localized heating and elevated extracellular ROS levels, resulting in bacterial inactivation. Also, the Mo^{4+} ions released from the platform penetrated the bacterial membrane, triggering intracellular ROS generation and depletion of intracellular GSH, further contributing to bacterial eradication. The 2D bio-HJs produced localized heating and elevated extracellular ROS levels upon NIR laser irradiation, leading to bacterial deactivation. Simultaneously, Mo^{4+} ions easily penetrated the ruptured bacterial membrane, triggering intracellular ROS and depleting intracellular GSH.

In the "ROS Hurricane", bacteria faced substantial destruction from internal and external sources. However, when supplemented with fibroblast growth factor-21 (FGF21), 2D bio-hybrid junctions (bio-HJs) demonstrated favorable compatibility with cells and enhanced cell movement in vitro. Scheibe et al. [105] emphasized the necessity of conducting an in vitro examination to assess the impact of various types of MXenes and their precursors on human cell lines within the framework of nanomaterial safety. To this end, a range of multi-layered, few-layered, and single-layered $Ti_3C_2T_x$, alongside TiC, Ti_2AlC, and Ti_3AlC_2, were synthesized. Following the trends in nanomaterial safety assessment, thorough characterization encompassing morphology, size purity, and surface charge was conducted (**Figure 23**). Subsequently, various biological responses (including cytotoxicity, membrane permeability, reactive oxygen species generation, and mechanical stress) induced by MXenes, TiC, and parental MAX phases were investigated and compared using human fibroblasts (MSU1.1) and cervical cancer cells (HeLa) as model systems, reflecting differing tumorigenic properties.

The findings indicated that exposure to elevated concentrations ($\geq$400 μg/mL) of TiC, Ti_2AlC, and Ti_3AlC_2 particles, sized < 44 μm, could pose significant harm, eliciting pronounced cytotoxic effects through oxidative and mechanical stress mechanisms. Conversely, all forms of $Ti_3C_2T_x$ were deemed safe for MSU1.1 cells, exhibiting only minor cytotoxic tendencies at the highest concentration levels. Furthermore, the observed cytotoxic behaviors were contingent upon cell type, with greater susceptibilities observed in cancer-derived cells.
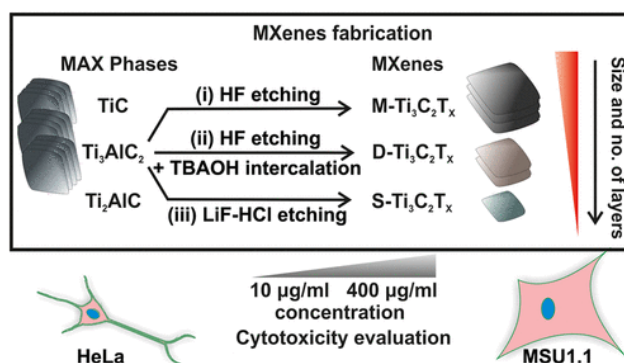

Figure 23. Cytotoxicity assessment of Ti-Al-C based MAX phases and $Ti_3C_2T_x$ MXenes on human fibroblasts and cervical cancer cells [105].

5.13. MXene-based materials for tissue engineering

2D MXenes are being used in the fields of tissue engineering and regenerative medicine. Also, because of their good electrical behavior, MXenes are used for neural tissue regeneration. Establishing artificial conduits to facilitate the growth of regenerating nerves and guide them through damaged areas is imperative for neuronal restoration. Despite the historical use of various natural and synthetic polymers in neural tissue engineering, certain drawbacks persist [106]. For instance, while poly (3,4-ethylene dioxythiophene) exhibits commendable biocompatibility and sufficient electrical and chemical stability, its proclivity towards chronic inflammation and limited degradability render it an unsuitable candidate.

Presently, MXenes are being incorporated as additives into polymeric nanofibers, fostering the growth of supportive cells and endowing them with sustained neurotrophic properties [107]. To validate the efficacy of MXene-modified polylactic acid nanofibers in facilitating nerve-guiding path formation, an experimental study was conducted. Integration of MXenes notably augmented the electrical conductivity of the material. The resultant current flow in the modified nanofiber membrane remained below 150 mA under an applied voltage of 5.5 V, although higher potentials induced dielectric behavior in the fabricated nanofibers. These findings underscore the potential of MXenes in conferring electroconductivity to polymer membranes for neural tissue engineering applications. Notably, the presence of polylactic acid membranes containing immobilized MXenes did not exhibit adverse effects on cellular viability, as evidenced by resazurin reduction assays. However, the outcomes were partially satisfactory due to challenges associated with MXene immobilization and handling during cell culture. Furthermore, the composite material demonstrated promising anti-adhesive properties against bacterial colonization, potentially disrupting cellular morphology and membrane integrity.

6. Challenges and future prospects

The numerous studies on MXenes and scientific reports, conferences, and articles are growing day by day, and the research in the right direction may address all challenges and issues. The possible right direction to the current state-of-art can open up new opportunities for innovations and developments of MXene-based devices. The current cutting-edge research on water-related issues can address the real problems, and the remarkable properties can make these efforts successful [3,9–13,73]. MXenes are mostly designed using the top-down approach, while very few reports on the bottom-up approaches are available in the literature [11,72]. Serious efforts are needed to explore the hidden potential in the bottom-up approaches to the synthesis of MXenes, to improve the characteristic properties of the MXenes, and to obtain desirable forms and structures of MXenes. After almost a decade of discovery of MXenes, this remarkable progress has been observed in the many fields and aspects related to MXenes, for example, synthesis, structural patterns, more applicability, and the discovery of new MXene compounds. But still, there are challenges left. The major challenges remain for MXenes and the application of MXene-based materials. Very few MAX phases have been experimentally exfoliated

to date, while a few dozen possibilities are predicted. Theoretically, the MXenes can be the best possible cathode for high energy density 3458 Wh kg^{-1} Li-air batteries, but there is no successful report regarding this aspect [108,109]. Recently, Zn-air batteries have been successfully reported with promising performance, which proves the potential of MXenes [106,107].

Most of the reports are about coin-cell-based devices; it is just to see the actual potential of the material, while the pouch-type or large assembly of cells is needed to be tested for futuristic flexible, printable, or wearable applications of MXene-based batteries and supercapacitors. The performance of MXene-based devices with solid electrolytes needs to be tested to confirm the possibility of flexible and wearable MXene-based devices [61,110]. MXenes are proposed to be the future materials for absorption of toxic pollutants, but they need to be exploited fully [111]. For example, one of the promising MXene K_xMeO_2-based electrodes for batteries is under investigation, while the existing report shows lower operating potential and lower energy density in comparison to graphite/$LiMn_2O_4$-based LIBs [112] (**Figure 24**).
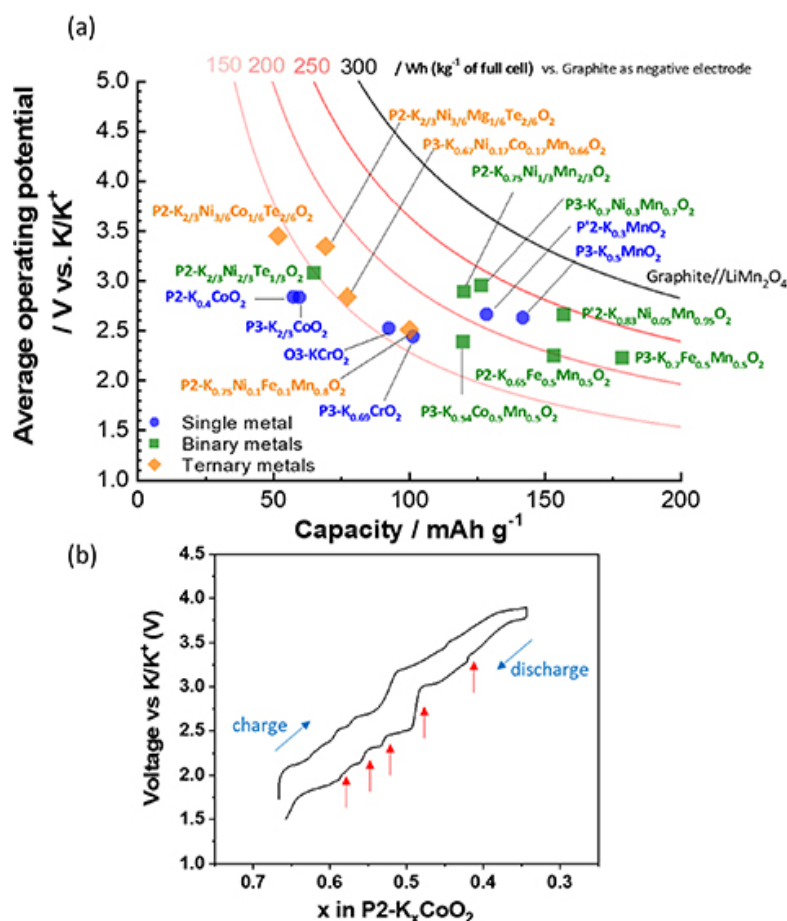
Figure 24. (a) Average operating potential versus gravimetric capacity plot for selected layered TMOs for PIBs; **(b)** typical charge/discharge curve for P2-type K_xCoO_2Xu [112].

The operating potential and capacity values reported for the various battery cells are derived from the potentiated state in half cells. While calculating the energy densities of full cells, graphite (with a capacity of 279 mAhg^{-1} at 0.25 V vs. K/K$^+$) is

employed as the negative electrode material in conjunction with various positive electrode materials. The key latest developments in MXene and MXene-based materials and devices are presented. Some key challenges and issues related to MXene-based materials for various applications need to be taken up [112].

7. Conclusion

MXene and MXene-based materials can be synthesized through various approaches and methodologies tailored to meet some specific properties and structural specification requirements. The exponential growth in the research articles and expansion of research groups around the world suggests expected tremendous improvement in the synthesis techniques soon. The specific properties of MXenes and MXene-based materials, e.g., specific surface area, chemical stability, hydrophilicity, thermal conductivity, and environmental compatibility, can be modified and customized according to the needs of applications. Water purification, absorption of impurities, metal removal, and degradation of impurities can be successfully done using MXenes-based materials in a better way. MXenes exhibit promising potential in diverse realms, including environmental remediation, biomedical applications, batteries, supercapacitors, and other advanced engineering fields. MXenes demonstrate excellent biocompatibility in biomedical applications. Nonetheless, there exist several challenges and unexplored research avenues that demand immediate attention to fully capitalize on the remarkable characteristics of these materials.

While numerous hurdles persist in translating research outputs into real-world applications, the growing research in many other fields with technological advancement is expected to conquer the existing challenges, and MXenes are anticipated to emerge as a pivotal component of futuristic applications, reflecting the continued evolution and integration of these intriguing materials into diverse domains.

Conflict of interest: The authors declare no conflict of interest.

References

1. Wang Y, Wang X, Li X, et al. Engineering 3D Ion Transport Channels for Flexible MXene Films with Superior Capacitive Performance. Advanced Functional Materials. 2019; 29(14). doi: 10.1002/adfm.201900326
2. Naguib M, Halim J, Lu J, et al. New two-dimensional niobium and vanadium carbides as promising materials for li-ion batteries. Journal of the American Chemical Society. 2013; 135(43): 15966–15969. doi: 10.1021/ja405735d
3. Okubo M, Sugahara A, Kajiyama S, Yamada A. MXene as a Charge Storage Host. Accounts of Chemical Research. 2018; 51(3): 591–599. doi: 10.1021/acs.accounts.7b00481
4. Wang H, Wu Y, Yuan X, et al. Clay-Inspired MXene-Based Electrochemical Devices and Photo-Electrocatalyst: State-of-the-Art Progresses and Challenges. Advanced Materials. 2018; 30(12). doi: 10.1002/adma.201704561
5. An H, Habib T, Shah S, et al. Surface-agnostic highly stretchable and bendable conductive MXene multilayers. Science Advances. 2018; 4(3). doi: 10.1126/sciadv.aaq0118
6. Zhan C, Naguib M, Lukatskaya M, et al. Understanding the MXene Pseudocapacitance. The Journal of Physical Chemistry Letters. 2018; 9(6): 1223–1228. doi: 10.1021/acs.jpclett.8b00200
7. Xiong D, Li X, Bai Z, et al. Recent Advances in Layered Ti_3C_2Tx MXene for Electrochemical Energy Storage. Small. 2018; 14(17). doi: 10.1002/smll.201703419

8. Anasori B, Xie Y, Beidaghi M, et al. Two-Dimensional, Ordered, Double Transition Metals Carbides (MXenes). ACS Nano. 2015; 9(10): 9507–9516. doi: 10.1021/acsnano.5b03591

9. Wang Y, Wang Y. MXene ink printing of high-performance micro-supercapacitors. Carbon Neutralization. 2021. doi: 10.1002/cnl2.165

10. Badawi N, Bhuyan M, Luqman M, et al. MXenes the future of solid-state supercapacitors: Status, challenges, prospects, and applicatio. The Arabian Journal of Chemistry .2024; 10(66). doi: 10.1016/j.arabjc.2024.105866

11. Kajiyama S, Szabova L, Sodeyama K, et al. Sodium-Ion Intercalation Mechanism in MXene Nanosheets. ACS Nano. 2016; 10(3): 3334–3341. doi: 10.1021/acsnano.5b06958

12. Vonlanthen D, Lazarev P, See KA, et al. A Stable Polyaniline-Benzoquinone-Hydroquinone Supercapacitor. Advanced Materials. 2014; 26(30): 5095–5100. doi: 10.1002/adma.201400966

13. Zhang C, Kremer MP, Seral-Ascaso A, et al. Stamping of Flexible, Coplanar Micro-Supercapacitors Using MXene Inks. Advanced Functional Materials. 2018; 28(9). doi: 10.1002/adfm.201705506

14. Kurra N, Ahmed B, Gogotsi Y, et al. MXene-on-Paper Coplanar Microsupercapacitors. Advanced Energy Materials. 2016; 6(24). doi: 10.1002/aenm.201601372

15. Xu S, Dall'Agnese Y, Wei G, et al. Screen-printable microscale hybrid device based on MXene and layered double hydroxide electrodes for powering force sensors. Nano Energy. 2018; 50: 479–488. doi: 10.1016/j.nanoen.2018.05.064

16. Zhang C, McKeon L, Kremer MP, et al. Additive-free MXene inks and direct printing of micro-supercapacitors. Nature Communications. 2019; 10(1). doi: 10.1038/s41467-019-09398-1

17. Jiao S, Zhou A, Wu M, et al. Kirigami Patterning of MXene/Bacterial Cellulose Composite Paper for All-Solid-State Stretchable Micro-Supercapacitor Arrays. Advanced Science. 2019; 6(12). doi: 10.1002/advs.201900529

18. Luo S, Xie L, Han F, et al. Nanoscale Parallel Circuitry Based on Interpenetrating Conductive Assembly for Flexible and High-Power Zinc Ion Battery. Advanced Functional Materials. 2019; 29(28). doi: 10.1002/adfm.201901336

19. Ma Y, Liu N, Li L, et al. A highly flexible and sensitive piezoresistive sensor based on MXene with greatly changed interlayer distances. Nature Communications. 2017; 8(1). doi: 10.1038/s41467-017-01136-9

20. Ronchi RM, Arantes JT, Santos SF. Synthesis, structure, properties and applications of MXenes: Current status and perspectives. Ceramics International. 2019; 45(15): 18167–18188. doi: 10.1016/j.ceramint.2019.06.114

21. Naguib M, Mashtalir O, Carle J, et al. Two-Dimensional Transition Metal Carbides. ACS Nano. 2012; 6(2): 1322–1331. doi: 10.1021/nn204153h

22. Naguib M, Mochalin VN, Barsoum MW, et al. 25th Anniversary Article: MXenes: A New Family of Two-Dimensional Materials. Advanced Materials. 2013; 26(7): 992–1005. doi: 10.1002/adma.201304138

23. Hemanth NR, Kandasubramanian B. Recent advances in 2D MXenes for enhanced cation intercalation in energy harvesting Applications: A review. Chemical Engineering Journal. 2020; 392: 123678. doi: 10.1016/j.cej.2019.123678

24. Mashtalir O, Naguib M, Mochalin VN, et al. Intercalation and delamination of layered carbides and carbonitrides. Nature Communications. 2013; 4(1). doi: 10.1038/ncomms2664

25. Shekhirev M, Shuck CE, Sarycheva A, et al. Characterization of MXenes at every step, from their precursors to single flakes and assembled films. Progress in Materials Science. 2021; 120: 100757. doi: 10.1016/j.pmatsci.2020.100757

26. Jain A, Ong S, Hautier G, et al. Commentary: The materials project: A materials genome approach to accelerating materials innovation. APL Materials.2013; 1(1). doi: 10.1063/1.4812323/119685

27. Lim GP, Soon CF, Ma NL, et al. Cytotoxicity of MXene-based nanomaterials for biomedical applications: A mini review. Environmental Research. 2021; 201: 111592. doi: 10.1016/j.envres.2021.111592

28. Shahmoradi S, Mirshafiei M, Zare I, et al. Two-Dimensional Nanomaterials-Based Polymer Nanocomposites for Tissue Engineering Applications. Scrivener Publishing LLC. 2024; 9781119904847. doi:10.1002/9781119905110.ch17

29. Sana SS, Santhamoorthy M, Haldar R, et al. Recent advances on MXene-based hydrogels for antibacterial and drug delivery applications. Process Biochemistry. 2023; 132: 200–220. doi: 10.1016/j.procbio.2023.06.022

30. Alyasi H, Wahib S, Gomez TA, et al. The power of MXene-based materials for emerging contaminant removal from water— A review. Desalinction. 2024, 117913. doi: 10.1016/j.desal.2024.117913

31. Ibrahim KB, Shifa TA, Zorzi S, et al. Emerging 2D materials beyond mxenes and TMDs: Transition metal carbo-chalcogenides. Progress in Materials Science. 2024, 101287. doi: 10.1016/j.pmatsci.2024.101287

32. Naguib M, Kurtoglu M, Presser V, et al. Two-Dimensional Nanocrystals Produced by Exfoliation of Ti_3AlC_2. Advanced Materials. 2011; 23(37): 4248–4253. doi: 10.1002/adma.201102306

33. Rafieerad A, Yan W, Sequiera GL, et al. Application of Ti_3C_2 MXene Quantum Dots for Immunomodulation and Regenerative Medicine. Advanced Healthcare Materials. 2019; 8(16). doi: 10.1002/adhm.201900569

34. Chen K, Chen Y, Deng Q, et al. Strong and biocompatible poly(lactic acid) membrane enhanced by Ti_3C_2Tz (MXene) nanosheets for Guided bone regeneration. Materials Letters. 2018; 229: 114–117. doi: 10.1016/j.matlet.2018.06.063

35. Pan S, Yin J, Yu L, et al. 2D MXene-Integrated 3D-Printing Scaffolds for Augmented Osteosarcoma Phototherapy and Accelerated Tissue Reconstruction. Advanced Science. 2019; 7(2). doi: 10.1002/advs.201901511

36. Cui Y, Liu M, Huang H, et al. A novel one-step strategy for preparation of Fe_3O_4-loaded Ti_3C_2 MXenes with high efficiency for removal organic dyes. Ceramics International. 2020; 46(8): 11593–11601. doi: 10.1016/j.ceramint.2020.01.188

37. Wychowaniec JK, Litowczenko J, Tadyszak K, et al. Unique cellular network formation guided by heterostructures based on reduced graphene oxide—Ti_3C_2Tx MXene hydrogels. Acta Biomaterialia. 2020; 115: 104–115. doi: 10.1016/j.actbio.2020.08.010

38. Wang H, Sun F, Zhao Y, et al. A highly luminescent organic crystal with the well-balanced charge transport property: The role of cyano-substitution in the terminal phenyl unit of distyrylbenzene. Organic Electronics. 2016; 28: 287–293. doi: 10.1016/j.orgel.2015.11.008

39. Rastin H, Zhang B, Mazinani A, et al. 3D bioprinting of cell-laden electroconductive MXene nanocomposite bioinks. Nanoscale. 2020; 12(30): 16069–16080. doi: 10.1039/d0nr02581j

40. He J, Yang J, Jiang F, et al. Photo-assisted peroxymonosulfate activation via 2D/2D heterostructure of Ti_3C_2/g-C_3N_4 for degradation of diclofenac. Chemosphere. 2020; 258: 127339. doi: 10.1016/j.chemosphere.2020.127339

41. Song H, Du R, Wang Y, et al. Anchoring single atom cobalt on two-dimensional MXene for activation of peroxymonosulfate. Applied Catalysis B: Environmental. 2021; 286: 119898. doi: 10.1016/j.apcatb.2021.119898

42. Ma Y, Xiong D, Lv X, et al. Rapid and long-lasting acceleration of zero-valent iron nanoparticles@Ti_3C_2-based MXene/peroxymonosulfate oxidation with bi-active centers toward ranitidine removal. Journal of Materials Chemistry A. 2021; 9(35): 19817–19833. doi: 10.1039/d1ta02046c

43. Wu Y, Xiong W, Wang Z, et al. Self-assembled MXene-based Schottky-junction upon Transition metal oxide for regulated tumor microenvironment and enhanced CDT/PTT/MRI activated by NIR irradiation. Chemical Engineering Journal. 2022; 427: 131925. doi: 10.1016/j.cej.2021.131925

44. Lee JB, Choi GH, Yoo PJ. Oxidized-co-crumpled multiscale porous architectures of MXene for high performance supercapacitors. Journal of Alloys and Compounds. 2021; 887: 161304. doi: 10.1016/j.jallcom.2021.161304

45. Xu S, Liu C, Jiang X, et al. Ti_3C_2 MXene promoted Fe_{3+}/H_2O_2 fenton oxidation: Comparison of mechanisms under dark and visible light conditions. Journal of Hazardous Materials. 2023; 444: 130450. doi: 10.1016/j.jhazmat.2022.130450

46. Li Q, Wang X, Chen L, et al. Cu/Cu_2O nanoparticles modified Ti_3C_2 MXene with in-situ formed TiO_{2-X} for detection of hydrogen peroxide. Ceramics International. 2023; 49(6): 9632–9641. doi: 10.1016/j.ceramint.2022.11.133

47. Zhu F, Wang X, Yang X, et al. Reasonable design of an MXene-based enzyme-free amperometric sensing interface for highly sensitive hydrogen peroxide detection. Analytical Methods. 2021; 13(22): 2512–2518. doi: 10.1039/d1ay00568e

48. Dekanovsky L, Huang H, Akir S, et al. Light-Driven MXene-Based Microrobots: Mineralization of Bisphenol A to CO_2 and H_2O. Small Methods. 2023; 7(8). doi: 10.1002/smtd.202201547

49. Ihsanullah I. MXenes (two-dimensional metal carbides) as emerging nanomaterials for water purification: Progress, challenges and prospects. Chemical Engineering Journal. 2020; 388: 124340. doi: 10.1016/j.cej.2020.124340

50. Dixit F, Zimmermann K, Dutta R, et al. Application of MXenes for water treatment and energy-efficient desalination: A review. Journal of Hazardous Materials. 2022; 423: 127050. doi: 10.1016/j.jhazmat.2021.127050

51. Rasool K, Pandey RP, Rasheed PA, et al. Water treatment and environmental remediation applications of two-dimensional metal carbides (MXenes). Materials Today. 2019; 30: 80–102. doi: 10.1016/j.mattod.2019.05.017

52. Hojjati-Najafabadi A, Mansoorianfar M, Liang T, et al. Magnetic-MXene-based nanocomposites for water and wastewater treatment: A review. Journal of Water Process Engineering. 2022; 47: 102696. doi: 10.1016/j.jwpe.2022.102696

53. Ihsanullah I. Potential of MXenes in Water Desalination: Current Status and Perspectives. Nano-Micro Letters. 2020; 12(1). doi: 10.1007/s40820-020-0411-9

54. Saththasivam J, Wang K, Yiming W, et al. A flexible Ti3C2Tx (MXene)/paper membrane for efficient oil/water separation. RSC Advances. 2019; 9(29): 16296–16304. doi: 10.1039/c9ra02129a

55. Bao W, Tang X, Guo X, et al. Porous Cryo-Dried MXene for Efficient Capacitive Deionization. Joule. 2018; 2(4): 778–787. doi: 10.1016/j.joule.2018.02.018

56. Tang X, Guo X, Wu W, et al. 2D Metal Carbides and Nitrides (MXenes) as High-Performance Electrode Materials for Lithium-Based Batteries. Advanced Energy Materials. 2018; 8(33). doi: 10.1002/aenm.201801897

57. Deng D. Li-ion batteries: basics, progress, and challenges. Energy Science & Engineering. 2015; 3(5): 385–418. doi: 10.1002/ese3.95

58. Goodenough JB. Evolution of Strategies for Modern Rechargeable Batteries. Accounts of Chemical Research. 2012; 46(5): 1053–1061. doi: 10.1021/ar2002705

59. Jyoti J, Singh BP, Sandhu M, et al. New insights on MXene and its advanced hybrid materials for lithium-ion batteries. Sustainable Energy & Fuels. 2022; 6(4): 971–1013. doi: 10.1039/d1se01681d

60. Wu X, Jovanović MR. Sparsity-promoting optimal control of systems with symmetries, consensus and synchronization networks. Systems & Control Letters. 2017; 103: 1–8. doi: 10.1016/j.sysconle.2017.02.007

61. Wang X, Kajiyama S, Iinuma H, et al. Pseudocapacitance of MXene nanosheets for high-power sodium-ion hybrid capacitors. Nature Communications. 2015; 6(1). doi: 10.1038/ncomms7544

62. Zhang P, Wang D, Zhu Q, et al. Plate-to-Layer Bi_2MoO_6/MXene-Heterostructured Anode for Lithium-Ion Batteries. Nano-Micro Letters. 2019; 11(1): 01.doi: 10.1007/s40820-019-0312-y

63. Zou G, Zhang Z, Guo J, et al. Synthesis of MXene/Ag Composites for Extraordinary Long Cycle Lifetime Lithium Storage at High Rates. ACS Applied Materials & Interfaces. 2016; 8(34): 22280–22286. doi: 10.1021/acsami.6b08089

64. Tian Y, An Y, Xiong S, et al. A general method for constructing robust, flexible and freestanding MXene@metal anodes for high-performance potassium-ion batteries. Journal of Materials Chemistry A. 2019; 7(16): 9716–9725. doi: 10.1039/c9ta02233c

65. Jiang T, Xiong Q, Yang H, et al. Performance and application of Si/Ti_3C_2T x (MXene) composites in lithium-ion battery. Journal of Physics: Energy. 2023; 5(1): 014020. doi: 10.1088/2515-7655/acb6b4

66. Zhang W, Shi H, Wang D, et al. Three-dimensional Ti_3C_2 MXene@silicon@nitrogen-doped carbon foam for high performance self-standing lithium-ion battery anodes. Journal of Electroanalytical Chemistry. 2022; 921: 116664. doi: 10.1016/j.jelechem.2022.116664

67. Rojas Dávalos CA. Chemomechanical study of silicon composite anodes for lithium-ion batteries. Available online: https://tesis.pucp.edu.pe/repositorio/handle/20.500.12404/21155 (accessed on 15 December 2021).

68. Lei D, Liu N, Su T, et al. Roles of MXene in Pressure Sensing: Preparation, Composite Structure Design, and Mechanism. Advanced Materials. 2022; 34(52). doi: 10.1002/adma.202110608

69. Peng L, Zhu Y, Chen D, et al. Two-Dimensional Materials for Beyond-Lithium-Ion Batteries. Advanced Energy Materials. 2016; 6(11). doi: 10.1002/aenm.201600025

70. Tang X, Zhou D, Li P, et al. MXene-Based Dendrite-Free Potassium Metal Batteries. Advanced Materials. 2019; 32(4). doi: 10.1002/adma.201906739

71. Wang D, Ga Y, LiuY, et al. First-Principles Calculations of Ti_2N and Ti_2NT_2 (T = O, F, OH) Monolayers as Potential Anode Materials for Lithium-Ion Batteries and Beyond. Journal of Physical Chemistry C. 2017; 121(24): 13025. doi: 10.1021/acs.jpcc.7b03057

72. Wang G, Zhang L, Zhang J. A review of electrode materials for electrochemical supercapacitors. Chem Soc Rev. 2012; 41(2): 797–828. doi: 10.1039/c1cs15060j

73. Alhabeb M, Maleski K, Anasori B, et al. Guidelines for Synthesis and Processing of Two-Dimensional Titanium Carbide (Ti3C2Tx MXene). Chemistry of Materials. 2017; 29(18): 7633–7644. doi: 10.1021/acs.chemmater.7b02847

74. Lukatskaya MR, Kota S, Lin Z, et al. Ultra-high-rate pseudocapacitive energy storage in two-dimensional transition metal carbides. Nature Energy. 2017; 2(8). doi: 10.1038/nenergy.2017.105

75. Ghidiu M, Lukatskaya MR, Zhao MQ, et al. Conductive Two-Dimensional Titanium Carbide 'Clay' with High Volumetric Capacitance. Available online: https://www.nature.com/articles/nature13970 (accessed on 2 September 2023).

76. Pomerantseva E, Bonaccorso F, Feng X, et al. Energy storage: The future enabled by nanomaterials. Science. 2019; 366(6468). doi: 10.1126/science.aan8285

77. Couly C, Alhabeb M, Van Aken KL, et al. Asymmetric Flexible MXene-Reduced Graphene Oxide Micro-Supercapacitor. Advanced Electronic Materials. 2017; 4(1). doi: 10.1002/aelm.201700339

78. Rakhi RB, Ahmed B, Hedhili MN, et al. Effect of Postetch Annealing Gas Composition on the Structural and Electrochemical Properties of Ti2CTx MXene Electrodes for Supercapacitor Applications. Chemistry of Materials. 2015; 27(15): 5314–5323. doi: 10.1021/acs.chemmater.5b01623

79. Wen Y, Rufford TE, Chen X, et al. Nitrogen-doped Ti3C2Tx MXene electrodes for high-performance supercapacitors. Nano Energy. 2017; 38: 368–376. doi: 10.1016/j.nanoen.2017.06.009

80. Levitt AS, Alhabeb M, Hatter CB, et al. Electrospun MXene/carbon nanofibers as supercapacitor electrodes. Journal of Materials Chemistry A. 2019; 7(1): 269-277. doi: 10.1039/c8ta09810g

81. Kim SJ, Koh HJ, Ren CE, et al. Metallic Ti3C2Tx MXene Gas Sensors with Ultrahigh Signal-to-Noise Ratio. ACS Nano. 2018; 12(2): 986–993. doi: 10.1021/acsnano.7b07460

82. Vasyukova IA, Zakharova OV, Kuznetsov DV, et al. Synthesis, Toxicity Assessment, Environmental and Biomedical Applications of MXenes: A Review. Nanomaterials. 2022; 12(11): 1797. doi: 10.3390/nano12111797

83. Huang M, Gu Z, Zhang J, et al. MXene and black phosphorus based 2D nanomaterials in bioimaging and biosensing: progress and perspectives. Journal of Materials Chemistry B. 2021; 9(26): 5195–5220. doi: 10.1039/d1tb00410g

84. Huang H, Jiang R, Feng Y, et al. Recent development and prospects of surface modification and biomedical applications of MXenes. Nanoscale. 2020; 12(3): 1325–1338. doi: 10.1039/c9nr07616f

85. Lee E, VahidMohammadi A, Prorok BC, et al. Room Temperature Gas Sensing of Two-Dimensional Titanium Carbide (MXene). ACS Applied Materials & Interfaces. 2017; 9(42): 37184–37190. doi: 10.1021/acsami.7b11055

86. Sinha A, Dhanjai, Zhao H, et al. MXene: An emerging material for sensing and biosensing. TrAC Trends in Analytical Chemistry. 2018; 105: 424–435. doi: 10.1016/j.trac.2018.05.021

87. Yin T, Cheng Y, Hou Y, et al. 3D Porous Structure in MXene/PANI Foam for a High-Performance Flexible Pressure Sensor. Small. 2022; 18(48). doi: 10.1002/smll.202204806

88. Wang X, Lu J, Lu S, et al. Health monitoring of repaired composite structure using MXene sensor. Composites Communications. 2021; 27: 100850. doi: 10.1016/j.coco.2021.100850

89. George SM, Kandasubramanian B. Advancements in MXene-Polymer composites for various biomedical applications. Ceramics International. 2020; 46(7): 8522–8535. doi: 10.1016/j.ceramint.2019.12.257

90. Yang X, Zhang C, Deng D, et al. Multiple Stimuli-Responsive MXene-Based Hydrogel as Intelligent Drug Delivery Carriers for Deep Chronic Wound Healing. Small. 2021; 18(5). doi: 10.1002/smll.202104368

91. Huang J, Li Z, Mao Y, et al. Progress and biomedical applications of MXenes. Nano Select. 2021; 2(8): 1480–1508. doi: 10.1002/nano.202000309

92. Mohajer F, Ziarani GM, Badiei A, et al. Advanced MXene-Based Micro- and Nanosystems for Targeted Drug Delivery in Cancer Therapy. Micromachines. 2022; 13(10): 1773. doi: 10.3390/mi13101773

93. Liu A, Liu Y, Liu G, et al. Engineering of surface modified Ti3C2Tx MXene based dually controlled drug release system for synergistic multi-therapies of cancer. Chemical Engineering Journal. 2022; 448: 137691. doi: 10.1016/j.cej.2022.137691

94. Dong Y, Li S, Li X, et al. Smart MXene/agarose hydrogel with photothermal property for controlled drug release. International Journal of Biological Macromolecules. 2021; 190: 693–699. doi: 10.1016/j.ijbiomac.2021.09.037

95. Zhang WJ, Li S, Vijayan V, et al. ROS- and pH-Responsive Polydopamine Functionalized Ti3C2Tx MXene-Based Nanoparticles as Drug Delivery Nanocarriers with High Antibacterial Activity. Nanomaterials. 2022; 12(24): 4392. doi: 10.3390/nano12244392

96. Wu Z, Shi J, Song P, et al. Chitosan/hyaluronic acid based hollow microcapsules equipped with MXene/gold nanorods for synergistically enhanced near infrared responsive drug delivery. International Journal of Biological Macromolecules. 2021; 183: 870–879. doi: 10.1016/j.ijbiomac.2021.04.164

97. Liu Y, Tian Y, Han Q, et al. Synergism of 2D/1D MXene/cobalt nanowire heterojunctions for boosted photo-activated antibacterial application. Chemical Engineering Journal. 2021; 410: 128209. doi: 10.1016/j.cej.2020.128209

98. Nguyen VH, Nguyen BS, Hu C, et al. Novel Architecture Titanium Carbide (Ti3C2Tx) MXene Cocatalysts toward Photocatalytic Hydrogen Production: A Mini-Review. Nanomaterials. 2020; 10(4): 602. doi: 10.3390/nano10040602

99. Koyappayil A, Chavan SG, Mohammadniaei M, et al. *β*-Hydroxybutyrate dehydrogenase decorated MXene nanosheets for the amperometric determination of *β*-hydroxybutyrate. Microchimica Acta. 2020; 187(5). doi: 10.1007/s00604-020-04258-y

100. Zhang J, Fu Y, Mo A. Multilayered Titanium Carbide MXene Film for Guided Bone Regeneration. International Journal of Nanomedicine. 2019; 14: 10091–10103. doi: 10.2147/ijn.s227830

101. Huang J, Su J, Hou Z, et al. The cytocompatibility of Ti3C2Tx MXene with Red Blood Cells and Human Umbilical Vein Endothelial Cells and the Underlying Mechanisms. Chemical Research in Toxicology. 2023; 36(3): 347–359. doi: 10.1021/acs.chemrestox.2c00154

102. Usman KAS, Yao Y, Bacal CJO, et al. Robust Biocompatible Fibers from Silk Fibroin Coated MXene Sheets. Advanced

Materials Interfaces. 2023; 10(9). doi: 10.1002/admi.202201634

103. Neubertova V, Guselnikova O, Yamauchi Y, et al. Covalent functionalization of Ti3C2T MXene flakes with Gd-DTPA complex for stable and biocompatible MRI contrast agent. Chemical Engineering Journal. 2022; 446: 136939. doi: 10.1016/j.cej.2022.136939

104. Yang Z, Fu X, Ma D, et al. Growth Factor-Decorated Ti3C2 MXene/MoS2 2D Bio-Heterojunctions with Quad-Channel Photonic Disinfection for Effective Regeneration of Bacteria-Invaded Cutaneous Tissue. Small. 2021; 17(50). doi: 10.1002/smll.202103993

105. Scheibe B, Wychowaniec JK, Scheibe M, et al. Cytotoxicity Assessment of Ti-Al-C Based MAX Phases and Ti3C2Tx MXenes on Human Fibroblasts and Cervical Cancer Cells. ACS Biomaterials Science & Engineering. 2019; 5(12): 6557–6569. doi: 10.1021/acsbiomaterials.9b01476

106. Amini S, Salehi H, Setayeshmehr M, et al. Natural and synthetic polymeric scaffolds used in peripheral nerve tissue engineering: Advantages and disadvantages. Polymers for Advanced Technologies. 2021; 32(6): 2267–2289. doi: 10.1002/pat.5263

107. Katz-Demyanetz A, Koptyug A, Popov VV. In-situ Alloying as a Novel Methodology in Additive Manufacturing. In: Proceedings of the 2020 IEEE 10th International Conference Nanomaterials: Applications & Properties (NAP). 2020. doi: 10.1109/nap51477.2020.9309652

108. Yi S, Liu G, Liu Z, et al. Theoretical insights into nitrogen fixation on Ti_2C and Ti_2CO_2 in a lithium-nitrogen battery. Journal of Materials Chemistry A. 2019; 7(34): 19950–19960. doi: 10.1039/c9ta06232g

109. Wei S, Wang C, Chen S, et al. Dial the Mechanism Switch of VN from Conversion to Intercalation toward Long Cycling Sodium-Ion Battery. Advanced Energy Materials. 2020; 10(12). doi: 10.1002/aenm.201903712

110. Wang C, Wei S, Chen S, et al. Delaminating Vanadium Carbides for Zinc-Ion Storage: Hydrate Precipitation and H_+/Zn_{2+} Co-Action Mechanism. Small Methods. 2019; 3(12). doi: 10.1002/smtd.201900495

111. Ming F, Liang H, Zhang W, et al. Porous MXenes enable high performance potassium ion capacitors. Nano Energy. 2019; 62: 853–860. doi: 10.1016/j.nanoen.2019.06.013

112. Zhong J, Sun W, Wei Q, et al. Efficient and scalable synthesis of highly aligned and compact two-dimensional nanosheet films with record performances. Nature Communications. 2018; 9(1). doi: 10.1038/s41467-018-05723-2